LMW-PTP modulates glucose metabolism in cancer cells

LMW-PTP modulates glucose metabolism in cancer cells.

Giulia Lori[§], Tania Gamberi[§], Paolo Paoli, Anna Caselli, Erica Pranzini, Riccardo Marzocchini, Alessandra Modesti and Giovanni Raugei*

Department of Experimental and Clinical Biomedical Sciences, University of Florence, Florence, Italy

[§] These authors contributed equally to the work.

* **Corresponding author:** Giovanni Raugei
email: giovanni.raugei@unifi.it
Address: viale G.B. Morgagni 50, 50134 Florence, Italy.
Telephone: +39 055 2751202
Fax: +39 055 4598305

Abstract

Background

Low Molecular Weight Phosphotyrosine Protein Phosphatase (LMW-PTP) is an enzyme involved not only in tumor onset and progression but also in type 2 diabetes. A recent review shows that LMW-PTP acts on several RTK (receptor tyrosine kinase) such as PDGFR, EGFR, EphA2, Insulin receptor. It is well described also its interaction with cSrc. It is noteworthy that most of these conclusions are based on the use of cell lines expressing low levels of LMW-PTP. The aim of the present study was to discover new LMW-PTP substrates in aggressive human tumors where the over-expression of this phosphatase is a common feature.

Methods

We investigated, by proteomic analysis, the protein phosphorylation pattern of A375 human melanoma cells silenced for LMW-PTP. Two-dimensional electrophoresis (2-DE) analysis, followed by western blot was performed using anti-phosphotyrosine antibodies, in order to identify differentially phosphorylated proteins.

Results

Proteomic analysis pointed out that most of the identified proteins belong to the glycolytic metabolism, such as **α-enolase, pyruvate kinase, glyceraldehyde-3-phosphate dehydrogenase and triosephosphate isomerase**, suggesting an involvement of LMW-PTP in glucose metabolism. Assessment of lactate production and oxygen consumption demonstrated that LMW-PTP silencing enhances glycolytic flux and slow down the oxidative metabolism. In particular, LMW-PTP expression affects PKM2 tyrosine-phosphorylation and nuclear localization, modulating its activity.

Conclusion

All these findings propose that tumor cells are subjected to metabolic reprogramming after LMW-PTP silencing, enhancing glycolytic flux, probably to compensate the inhibition of mitochondrial metabolism.

General significance

Our results highlight the involvement of LMW-PTP in regulating glucose metabolism in A375 melanoma cells.

Keywords

LMW-PTP; Glucose metabolism; PKM2; metabolic reprogramming of cancer cells.

1. Introduction

Low Molecular Weight Phosphotyrosine Protein Phosphatase (LMW-PTP) is an enzyme that has been recognized to play a dual role in the cell, being involved not only in tumor onset and progression but also in type 2 diabetes. As far as tumor is concerned, it has been reported that ectopic over-expression of LMW-PTP in NIH3T3 fibroblasts engrafted in nude mice leads to the formation of larger sarcomas [1]. Malentacchi et al., [2] demonstrated that LMW-PTP is over-expressed in different human cancers, such as colon cancer and neuroblastoma and, also in pre-neoplastic lesions of colon from rats treated with tumor inducing agents [3]. These data were recently further confirmed by a study on a wide collection of specimens from prostate cancer [4]. Interestingly, its over-expression, in many cases, correlates with a worse prognosis and a reduced survival. Moreover, it has been recently assessed that LMW-PTP is involved in the modulation of apoptosis and acquisition of drug resistance: over-expression of LMW-PTP confers resistance to vincristine in leukemic cells [5] and mediates malignant potential in colorectal cancer, inducing drug resistance and enhancing cell mobility [6].

Very recently Lori et al., [7], further confirmed the oncogenic role of LMW-PTP, suggesting the possibility of tumor treatment through LMW-PTP targeting: they demonstrated that using an inhibitor of LMW-PTP it is possible, in A375 and PC3 cancer cells (both over-expressing LMW-PTP) to enhance susceptibility to apoptosis induced by chemo-and radio-therapy. Together, these evidences sustain a clear oncogenic role of LMW-PTP.

As far as type 2 diabetes is concerned, it is known that Insulin Receptor (IR) is a substrate of LMW-PTP [8]. Being the IR negatively regulated by de-phosphorylation, it has been hypothesized that LMW-PTP may be involved in this disease. In a very recent paper it has been assessed that negative modulation of LMW-PTP in mice protect from fat-induced diabetes [9]. Another very recent paper [10] shows the ability of LMW-PTP to control the glycolytic phenotype in a specific leukemia cell line, suggesting that LMW-PTP may be involved also in the metabolic control of cancer cells.

Nowadays, many different substrates have been proposed for LMW-PTP, most of them collocated in a logical panorama of the different LMW-PTP functions. A recent review [11], shows the complexity of the LMW-PTP interactions in the cell, underlining particularly its action on several RTK (receptor tyrosine kinase), such as PDGFR, EGFR, EphA2, Insulin receptor and others. In addition, it is well described also its interaction with cSrc.

It should be noticed that most of the results were obtained using cell lines not expressing high levels of LMW-PTP. Our idea was to use the A375 cell line, derived from a very aggressive human melanoma, and expressing very high level of LMW-PTP. In this way, we aimed to select new LMW-PTP substrates, particularly important in tumors over-expressing this tyrosine phosphatase.

To this purpose, we performed comparative phospho-proteomic analysis between A375 control cells and cells silenced for LMW-PTP, to detect hyper-phosphorylated proteins, as putative targets of LMW-PTP enzymatic activity. Our results pointed out an interesting aspect of LMW-PTP functions, underling that this enzyme may have an important role in regulating oxidative metabolism in cancer cells.

2. Materials and Methods

2.1. Cell lines and transfection.

A375, PC3, HT29, DU145 and MEC1 cells were purchased from ATCC (Manassas, USA). Leukemia cells were cultured in Roswell Park Memorial Institute (RPMI 1640, Sigma-Aldrich, St. Louis, USA). A375, PC3, HT29 and DU145 were cultured in Dulbecco's Modified Eagles Medium (Euroclone). All media were supplemented with 10% fetal bovine serum, 100 U/ml penicillin, 100 mg/ml streptomycin (Sigma-Aldrich, St. Louis, USA). Cell lines were routinely tested for Mycoplasm infection using Mycoalert, Mycoplasma Detenction Kit (Lonza). 1x105 cells/mL were grown for 24h and then transiently transfected with LMW-PTP siRNA (Target sequence CCCATAGTGCACACTTGTATA, final concentration 20 nm), using Hiperfect Trafection Reagent (Qiagen) according to the manufacturer's instructions. To test the specificity of LMW-PTP transfection, control cells were transfected with a Scramble Sequence (AllStars Negative Control siRNA, final concentration 20nM, Qiagen). DU145 cells were transiently transfected with pRcCMV-C12S-LMW-PTP expressing the dominant-negative (Dn) Cys-12 to Ser mutant of LMW-PTP (Chiarugi et al., 1995). Briefly, 10 μg of plasmidic DNA was transfected using Lipofectamine 2000 (Invitrogen) according to the manufacturer's instructions.

2.2. Western blotting

Cells were lysed on iced in 1X Laemmli buffer (0.5 M TrisHCl pH 6.8, 10% SDS, 20% glycerol, β-mercaptoethanol, 0.1% bromophenol blue) and samples were boiled for 10 minutes. Cell extracts were resolved by SDS-PAGE and transferred to PVDF membranes (BioRad). Membranes were incubated overnight at 4°C with the appropriate primary antibody: rabbit polyclonal anti-LMW-PTP were produced in our laboratory [7]. Annexin A1, PKM2, TIPS, GAPDH, α-Enolase, GLUT-1, Hexokinase II, Lamin A/C and Actin were obtained from Santa Cruz Biotechnology. Anti-phosphotyrosine, clone 4G10 were from Merck-Millipore. After washing in TPBS-Tween 20 (0.1%) membranes were incubated with the appropriate horseradish peroxidase-conjugated secondary antibodies (Santa Cruz Biotechnology) for 1h. Proteins were detected using Clarity Western ECL (Biorad) by UVP ChemiDoc-it 500 Imaging System (DBA Analytik Jena US).

2.3. Immuno and co-immunoprecipitation

Cells ($3x10^5$) were seeded in 60 mm plates and transfected with LMW-PTP siRNA or Dn mutant. After 28 h, cells were lysed for 20 min on ice in 300 µL of RIPA buffer (50mM TrisHCl pH 7.5, 150 mM NaCl, 100 mM NaF, 2 mM EGTA, 1% triton X-100, 10µL/ml protease and phosphatase inhibitor, Sigma). Lysates were centrifugated at 4°C, 14000 rpm for 15 min: supernatants were collected. After protein quantification with Bradford Assay, 400 µg of proteins were immunoprecipitated overnight, at 4°C with the specific primary antibodies (1:100). Then Protein A/G PLUS-Agarose (Santa Cruz) was added and incubated at 4°C for 1h. Immunocomplexes were collected and analyzed by western blotting.

2.4. Extracellular Flux (XF) analysis (Seahorse technology)

The Oxygen Consumption Rate (OCR, pmolesO_2 consumed/min) and the ExtraCellular Acidification Rate (ECAR, mpH/min) were determined by using the XF96 Extracellular Flux Analyzer (Seahorse Bioscience) according to manufacturer's instructions. Cells were plated 1.5×10^4 cells/well on XF96-well microplates in standard medium. After one-day incubation, were washed three times with an unbuffered assay medium (pH 7.4) and conditioned for 1 h at 37°C without CO_2. After incubation, XF measurements was performed. A Seahorse XF Cell Mito Stress Test was used to evaluate the mitochondrial function in different experimental conditions. Using this kit, parameters of mitochondrial function were determined by directly measuring the OCR of cells after the injection of specific drugs that target components of the ETC in the mitochondria. The compounds (oligomycin, FCCP, and a mix of rotenone and antimycin A) were injected in sequence to measure basal respiration, ATP–linked respiration, maximal respiration, and non-mitochondrial respiration, respectively. Maximal respiratory capacity was then calculated by subtracting the basal respiration values from maximal respiration values.

2.5. Lactate assay

Measurement of lactate production was determined using L-Lactic Acid (L-Lactate) colorimetric assay from Megazyme, according to manufacturer's instruction. Briefly, medium culture was collected and incubated in a buffer containing NAD+, D-GTP, and L-LDH. Measurements were done at 340 nm by using a spectrophotometer.

2.6. Glucose uptake

Cells ($1.8 \text{ X } 10^6$) were seeded in 35 mm dishes and transfected with siRNA. After 28 h, 1 µL /ml µCi/mL (U-14C) deoxy-D-Glucose (PerkinElmer) was added and dishes were incubated for 30 min

at 37°C. Then cells were washed twice with cold PBS and lysed with 0,1M NaOH. The amount of (U-14C) deoxy-D-Glucose incorporated was evaluated by a scintillator analyzer (Tri-Carb 2800TR, PerkinElmer).

2.7. Gelatin zymography

Conditioned media were collected and subjected to electrophoresis on 7.5% PAGE gels containing 0.1% gelatin. After electrophoresis the gel was washed twice with 2.5% triton X-100 and once with Reaction Buffer (50mM Tris HCl, pH 7.5, 200 mM NaCl, 5mM CaCl2). The gel was incubated overnight at 37°C with fresh Reaction Buffer. Then gel was stained with 0.25 Coomassie Brilliant Blue and destained (30% methanol and 10% acetic acid).

2.8. Boyden Chamber assay

Cell invasion was performed with 5 x 10^4 cells on 8-μm-pore Transwells (Corning) coated with 50 μg/cm2 of reconstituted Matrigel. Cells were harvest, resuspended in serum-free medium and placed in the upper compartment. In the lower chamber, 600 μL of medium supplemented with FBS was added as a chemoattractant. After the cells were incubated for 12 h at 37 ℃ in a 5% CO2 atmosphere. Cells adhering to the lower surface were stained with Diff Quick staining kit. The numbers of cells in 6 randomly selected fields in each well were counted.

2.9. Two-dimensional electrophoresis (2-DE)

A375 cells (3x10^5) were seeded in 100 mm plates and transfected with LMW-PTP siRNA or a scramble sequence (control cells) as described above. After 28 h, cells were lysed for 20 min on ice in 1 mL of RIPA buffer (50mM TrisHCl pH 7.5, 150 mM NaCl, 100 mM NaF, 2 mM EGTA, 1% triton X-100, 10μL/ml protease and phosphatase inhibitor, Sigma). Lysates were centrifuged at 4°C, 8000g for 15 min and then supernatants were collected. The cells were sonicated (15 s) and protein extracts were clarified by centrifugation at 8000g, 4°C for 15 min. For the first-dimension electrophoresis, protein samples (80 μg for Phospho-blots and 180 μg for Coomassie-stained gels) were applied to 110-mm pH 3–10 IPG® ReadyStrip (Bio-Rad, Hercules CA). The strips were then actively rehydrated in the protein isoelectric focusing (IEF) cell (Bio-Rad) at 50 V for 18 h. The isoelectric focusing was performed in increasing voltages as follows; 300 V for 1 h, then linear gradient to 8000 V for 5 h and finally 20 000 V/h. For the second dimension, the IPG® Strips, were equilibrated for 10 min in 50 mM Tris–HCl (pH 6.8) containing 6 M urea, 1% (w/v) sodium dodecyl sulfate (SDS), 30% (v/v) glycerol, and 0.5% dithiothreitol, and then re-equilibrated for 15 min in the same buffer containing 4.5% iodoacetamide instead of dithiothreitol. Linear gradient

precast criterion Tris–HCl gels (8–16%) (Bio-Rad) were used to perform second dimension electrophoresis. Precision Protein™ Standards (Bio-Rad, CA) were run along with the samples at 200 V for 65 min. For each sample (A375 cells transfected with LMW-PTP siRNA or the scramble sequence) two 2-DE gels were performed. Gels with 180 μg of protein samples were stained by colloidal Coomassie [12] to visualize protein spots; gels with 80 μg of protein samples was used to phosphoprotein detection by western blot analysis.

2.10. Immunodetection of tyrosine-phosphorylated proteins (2-D Phospho-blot)

After running, 2-DE gels, with 80 ug of protein sample, were blotted on polyvinylidene fluoride (PVDF) membrane. The PVDF membranes were incubated for 3 h at 4°C with the primary anti-phosphotyrosine 4G10 IgG antibody (1:1,000 dilution). An enhanced chemiluminescence kit (GE Healthcare) was used for detection by UVP ChemiDoc-it 500 Imaging System (DBA Analytik Jena US).

For each cell specimen (A375 cells transfected with LMW-PTP siRNA or the scramble sequence) three independent 2-DE experiments (both 2-DE colloidal Coomassie-stained gels and 2-D phospho-blots) were performed (biological replicates). To minimize the variability between the samples, from each 2-DE experiment, we carried out two technical replicates (two 2-DE colloidal Coomassie- stained gels and two 2-D phospho-blots). Then, for each cell specimen a total of six colloidal Coomassie-stained gels and six 2-D phospho-blots were analyzed. 2-DE gel and phospho-blots images were digitized using the Epson expression 1680 PRO scanner and saved with a resolution of 300 dpi and as 16-bit TIFF format. Computer-aided 2D image analysis was carried out using ImageMaster 2D Platinum software v7.0 (GE Healthcare) on both 2-D colloidal Coomassie gels (for differential expression analysis) and on 2-D phospho-blots (for differential phosphorylation analysis). After automatic protein detection and matching, the gels were manually corrected to remove wrongly assigned or duplicated spots and image artifacts. Relative spot volume (%V =V single spot/V total spots, where V is the integration of the optical density over the spot area) was used during analysis to reduce experimental error. Spots detected in the 2-D phospho-blots and 2D-colloidal Coomassie-stained gels were matched by computer-assisted image analysis using ImageMaster 2D Platinum v7.0 software. Phosphorylation index was then calculated as the ratio between the %V of phosphorylated spots on phospho-blots divided by the %V of their respective spots visualized on colloidal Coomassie-stained gels.

All statistical analysis was performed using a two-tailed Student's t-test. $P < 0.05$ was considered statistically significantly different. Protein spots with statistically altered immunoreactivity were

subjected to mass spectrometry (MS) analysis after excision of the matching spot on the gel stained with colloidal Coomassie [12].

2. 11. In gel digestion and peptide mass fingerprinting

For peptide mass fingerprinting (PMF) electrophoretic spots were manually excised and subjected to in gel digestion by addiction of trypsin using an in-gel digestion protocol previously described [13]. Protein identification was carried out by peptide mass fingerprinting (PMF) on an Ultraflex III MALDITOF/TOF mass spectrometer (Bruker Daltonics) equipped with a 200 Hz smartbeamt I laser. MS analysis was performed in the positive reflector mode according to defined parameters, as follows: 80 ns of delay; ion source 1: 25 kV; ion source 2: 21.75 kV; lens voltage: 9.50 kV; reflector voltage: 26.30 kV; and reflector 2 voltage: 14.00 kV. The applied laser wavelength and frequency were 353 nm and 100 Hz, respectively, and the percentage was set to 46%. Final mass spectra were produced by averaging 1500 laser shots targeting five different positions within the spot. Spectra were acquired automatically and the Flex Analysis software v3.0 (Bruker) was used for their analysis and for the assignment of the peaks. The applied software generated a list of peaks up to 200, using a signal-to-noise ratio of 3 as the threshold for peak acceptance. Recorded spectra were calibrated using, as the internal standard, peptides arising from trypsin auto-proteolysis. The mass lists were filtered for contaminant removal: mass matrix-related ions, trypsin auto-lysis and keratin peaks. Protein identification by Peptide Mass Fingerprint search was established using MASCOT search engine version 2.1 (Matrix Science, London, UK, http://www.matrixscience.com) through the UniProtKB database (http://www.uniprot.org/). Taxonomy was limited to Homo sapiens, a mass tolerance of 100 ppm was allowed, and the number of accepted missed cleavage sites was set to one. Alkylation of cysteine by carbamidomethylation was considered a fixed modification, while oxidation of methionine was considered as a possible modification. The criteria used to accept identifications included the extent of sequence coverage, the number of matched peptides, and a probabilistic score of $p < 0.05$. The PMF was performed for three LMW-PTP siRNA 2-DE gels, obtaining the same results.

2. 12. RNA Preparation and Quantitative Real Time PCR

Total RNA was extracted with RNeasy mini kit (Qiagen). Reverse transcription polymerase first-strand cDNA synthesis was performed by using the iScript cDNA synthesis Kit (Bio-Rad). RT-PCR was performed by using the SsoAdvanced Universal SYBR Green Supermix (BioRad) and specific primers for genes of interest. Primer sequences used for RT-PCR analysis are shown in Table 1. Analyses were performed with Rotor Gene-Q (Qiagen). PCR cycling conditions were: 95 °C for 30

sec, 96 °C for 15 sec, 40 cycles at 60°C. Data were expressed as Ct values and used for the relative quantification of targets with the ΔΔCt calculation.

3. Results

3.1. Tyrosine phosphorylation pattern and LMW-PTP

In order to discover new possible cellular substrates of LMW-PTP in aggressive human tumors, we investigated, by proteomic analysis, the protein phosphorylation pattern of A375 human melanoma cells silenced for LMW-PTP. As a preliminary experiment, we carried out a time course analysis of LMW-PTP protein level, 18, 28 and 36 hours after siRNA administration. With a western blot analysis, we determined that minimal LMW-PTP level was reached 28 h after siRNA transfection (Fig.1). All further experiments were carried out using this timing when the level of LMW-PTP is reduced to 20% with respect to control.

Proteomic analysis was performed comparing the protein tyrosine phosphorylation level of LMW-PTP silenced A375 cells with respect to scrambled siRNAs-treated control cells. 2-DE analysis, followed by western blot (Phospho-blot), was performed using anti-phosphotyrosine antibodies. Fig.2 shows representative images of the 2-D phospho-blots obtained from scramble (panel A) and silenced cells (panel B) including the corresponding colloidal Coomassie-stained gels (panel C, scramble, and panel D, silenced). Phospho-blot images were analyzed using ImageMaster 2D Platinum v7.0 software (GE-Healthcare). The normalization of immune-reactive spots was performed against their respective on the colloidal Coomassie-stained 2-DE gel images. We compared normalized-volume percentage values (%V) of spots on phospho-blots of silenced cells with those phospho-blots obtained from scramble cells. Statistical analysis, performed by two-tailed non-paired Student's t-test using Graphpad Prism 6 software, revealed 8 statistically differentially phosphorylated protein spots. These protein spots are circled in Fig.2.

3.2. Mass spectrometry identification of tyrosine-phosphorylated proteins

To identify significant phosphorylated protein spots, we performed preparative 2-DE gels, which were then colloidal Coomassie-stained. The phospho-blot images were matched to the corresponding colloidal Coomassie stained 2-DE gels and the spots corresponding to phosphorylated proteins were cut and subjected to MALDI-TOF mass spectrometry analysis. We successfully identified the eight protein spots whose tyrosine-phosphorylation level was increased in silenced LMW-PTP cells. The results of mass spectrometry identification are reported in Table 1, together with the corresponding spot numbers, score and coverage values of MALDI-TOF analysis, fold change in phosphorylation level and Student t-test p-value. Most of the identified proteins

belong to carbohydrate metabolism such as α-enolase (ENO1), pyruvate kinase (PKM2), glyceraldehyde-3-phosphate dehydrogenase (GAPDH) and Triosephosphate isomerase (TPIS). We also found an increase in the tyrosine-phosphorylation level of Annexin A1 (ANXA1) and Prelamin-A/C (LMNA). Concerning LMNA, it was identified in three different protein spots (spot 1, 2, 3). These spots display the same molecular weight but differ for the isoelectric point (pI). The observed pI (calculated using Progenesis SameSpots 4.0 software) of spot 2 corresponds to the theoretical pI of LMNA (6.57 by www.uniprot.org). The spot 1 shows an observed pI of 6.38 and the spot 3 of 6.85 thus suggesting the presence of different post-translationally modified forms of LMNA.

3.3. Validation of the proteomic analysis results

To confirm that the selected proteins are actually phosphorylated in tyrosine in an LMW-PTP-dependent manner, we performed an immunoprecipitation assay. A375 control cells (transfected with scrambled siRNA) and cells silenced for 28 h with LMW-PTP-specific siRNA, were lysed. Samples were separately immunoprecipitated with antibodies specific for the selected proteins, namely PKM2, ENO1, GAPDH, TPIS, Annexin 1 and Prelamin-A/C. Immunoprecipitated samples were subjected to western blot analysis using anti-phosphotyrosine antibodies, to evaluate the level tyrosine-phosphorylation of the selected proteins. Western blot images were analyzed with Kodak MI software. The results shown in Fig.3 (panels A to F) point out that all the selected proteins are over-phosphorylated when LMW-PTP is silenced, in line with the data obtained by the proteomic analysis.

3.4. LMW-PTP directly interacts with the selected proteins

To assess whether the six selected proteins may be substrates of LMW-PTP, we performed a co-immunoprecipitation assays, to evaluate a direct association between LMW-PTP and the putative substrates. To maximize the results, in this experiment we used a different human cell line, the prostate carcinoma DU145. These cells, expressing limited amount of LMW-PTP, were transfected with a vector expressing a dominant-negative form of LMW-PTP*(Dn)* [14] which is a mutant carrying a modification in a critical cysteine residue, present in the active site. This mutant is able to interact with substrates, but it cannot catalyze any tyrosine de-phosphorylation. Lysates of mock-transfected cells and of cells transfected with the *Dn* form of LMW-PTP were subjected to immunoprecipitation with antibodies against the six selected proteins. The immuno-precipitates were analyzed by western blot, using anti-LMW-PTP antibodies. Results are shown in Fig.3, panel G. In the cells overexpressing the dominant negative form of LMW-PTP the interactions are very

strong for all the six selected proteins. The interactions however, are evident, although at a lower extent, also in the mock transfected cells where LMW-PTP level is lower. This fact may indicate that the interaction is quite strong. Based on these evidences we can conclude that the six proteins are *bona fide* substrates of LMW-PTP. To demonstrate the specificity of these results, a co-immunoprecipitation control with an irrelevant antibody (GM130, Santa Cruz Biotechnology SC-16268) was performed. As expected a negative result was achieved (data not shown).

3.5. LMW-PTP modulates oxidative metabolism in different tumor cell lines.

For further analyses we decided to concentrate our attention on four of the six proteins selected by proteomic analysis involved in glucose metabolism. PKM2, GAPDH, ENO1 and TPIS are in fact all part of the glycolytic pathway, suggesting that LMW-PTP may be involved in the regulation of energetic metabolism in cancer cells. To go deeper in the possible role of LMW-PTP in the oxidative metabolism, we performed several different experiments. First, we evaluated the short-term effects of LMW-PTP downregulation on energetic metabolism of A375 cells. For this purpose, A375 cells were treated with Morin, a LMW-PTP inhibitor that triggers rapid and specific LMW-PTP degradation [7]. After 4 hours of incubation, the A375 cells were analyzed using Seahorse technology. We observed that Morin treatment causes a relevant decrease of glycolytic flux and of oxygen consumption (Fig.4). Based on the above results, we speculate that this effect is in large part due to PKM2 inhibition. Indeed, it is evident that LMW-PTP, hydrolyzing phosphotyrosine residues, contributes to maintain PKM2 in its active form. Conversely, LMW-PTP inhibition or down-regulation favors PKM2 phosphorylation/inhibition, slowing down glycolytic pathway, Krebs cycle, and reducing oxygen consumption rate. Phosphorylated form of PKM2 moves in the nucleus where it stimulates activity of transcription factor HIF-1α. This promotes transcription of glycolytic genes, contributing to the shift away from oxidative towards glycolytic metabolism. To strengthen the claim that PKM2 phosphorylation pattern is responsible for the observed effects on energy metabolism, we evaluated PKM2 phosphorylation levels after treatment with Morin by immunoprecipitation analysis. The results are reported in the Figure 4 (panel E, F). We found that treatment with Morin increased PKM2 phosphorylation levels, thereby confirming that 4 hours treatment are enough to enhance the phosphorylation status of PKM2.

In agreement with this result, we observed a partially different long-term effect due to LMW-PTP silencing: in these conditions cells show an enhanced glycolytic flux, and a high lactate production rate, but they consume lower oxygen and produce lower ROS levels with respect to control cells (Fig. 5). Together, these short and long-term effects support the hypothesis that tumor cells are

subjected to metabolic reprogramming after LMW-PTP silencing, enhancing glycolytic flux, probably to compensate for the loss of ATP caused by the OXPHOS inhibition.

In order to assess that LMW-PTP effects on energy metabolism are not restricted to the A375 cell line, we repeated the same experiments (as described in Fig. 5, panels A to C) on three different human tumor cell lines. We used PC3 (prostate cancer), HT29 (colon cancer) and MEC-1 (B-cell leukemia) cell lines. In Fig. S1, S2 and S3 we present the results for each cell line. In each panel A we show the effect of LMW-PTP silencing, 28 hours after siRNA administration, demonstrating a comparable efficiency with respect to the A375 cells (see Fig.1). In panels B, C and D respectively we present the evaluation of glucose uptake, lactate production and the rate of oxygen consumption in controls and LMW-PTP silenced cells, demonstrating that the effects are in any case qualitatively identical to those obtained using A375 cells. As far as glucose uptake and lactate production is concerned, a more pronounced effect can be observed for the PC3 cell line with respect to the other cell lines.

3.6. Action of LMW-PTP on PKM2, GLUT1 and Hexokinase II

It is known that PKM2 may be regulated also in its expression levels [15]. In order to assess how LMW-PTP level may influence glucose utilization, we investigated whether the increase of glucose uptake may be due to enhanced level of the key glycolytic enzyme PKM2. For this purpose, we analyzed the expression level of PKM2 either in A375 cells, silenced or not for the LMW-PTP. The results show that, when LMW-PTP is downregulated with siRNA, the level of PKM2 is higher with respect to control cells (Fig.6, panel A and B). In the same experimental conditions, we also measured the expression level of the GLUT1 glucose transporter. As reported in Fig. 6, a clear increase of GLUT1 level was detected in LMW-PTP silenced A375 cells (Fig.6 panel A and C). Moreover, we investigated variations of the expression level of Hexokinase II, the first rate-limiting enzyme of glycolysis, upon LMW-PTP silencing. The result pointed out a clear increase in Hexokinase II level (Fig.6, panel A and D).

Pyruvate kinase controls the final and rate-limiting reaction of glycolysis and is present in the cell in different isoforms. In contrast to PKM1, which is present in a constitutively tetrameric active form, PKM2 undergoes conformational conversion between a tetrameric/full active and a dimeric/less active state [16, 17], able to translocate into the nucleus [18, 19]. We have determined whether LMW-PTP silencing may influence also the rate of PKM2 nuclear localization. In cells silenced for LMW-PTP, we can observe that the nuclear amount of PKM2 markedly increases with respect to the cytoplasmic one (Fig.6 panel E).

3.7. Action of LMW-PTP on cell motility

The increase of M2 isoform of pyruvate kinase versus M1 isoform have been correlated with higher cellular proliferation. In fact, PKM2 expression in tumor proliferating cells sustains Warburg metabolism [20, 21], leading to an increase of the glycolytic pathway. For this reason, we evaluated the proliferating rate of A375 cell s, transfected either with scramble or LMW-PTP specific siRNA. Fig.7 (panel A) shows that LMW-PTP silencing causes an increase of cell proliferation rate, followed up for 72h after transfection. Since high proliferative and glycolytic cancer cells show a lower EMT phenotype, we decided to analyzed the invasiveness of A375 melanoma cells upon LMW-PTP modulation. The results confirmed that, after LMW-PTP silencing, A375 cells are less able to invade through a Matrigel support (panel B), due to a decrease of MMP secretion (panel C), These conditions, as already shown, lead to an increase of glycolytic rate (see results of Fig. 5). To evaluate whether, in A375 cells, LMW-PTP silencing could affected transcription of EMT markers we analysed by using RT-PCR the mRNA expression levels of SNAIL, SLUG. As expected, we found that mRNA level of LMW-PTP strongly decreases 28 hours after transfection (Fig.7 panel D). At the same moment, we found that also mRNA expression levels of SNAIL (panel E), SLUG (panel F) decreased, while expression of E-cadherin mRNA levels increased (panel G). Conversely, no effects were observed after transfection of scrambles siRNA. Together, these results demonstrated that LMW-PTP silencing inhibits transcription of key factors involved in EMT, and stimulates expression of E-cadherin, reinforcing data previously reported in this paper.

4. Discussion

In this study, we performed a differential phospho-proteomic analysis of A375 cells, in order to identify possible new LMW-PTP substrates. Although several different substrates have been already defined for this phosphatase, a global analysis was not yet carried out. Moreover, since it is now clear that LMW-PTP over-expression in tumor cells correlates with higher aggressiveness, this analysis was carried out on the A375 human melanoma cell line, derived from a very aggressive tumor, expressing very high level of LMW-PTP. We found that six different proteins result to be over-phosphorylated on tyrosine residues upon LMW-PTP silencing, namely PKM2, GAPDH, α-enolase, TPIS, Lamin, and Annexin A1. For all the six selected proteins, it was possible to assess that it exists a direct molecular contact with the phosphatase, strongly suggesting that they are bona fide LMW-PTP substrates. Interestingly, our data show that four out of six of the new putative LMW-PTP substrates are glycolytic enzymes. These evidences suggest that LMW-PTP could have a key role in regulating the glycolytic pathway, probably by modulating the phosphorylation status of these enzymes.

As far as PKM2 is concerned, it is already known that the activity of this enzyme is modulated by tyrosine phosphorylation. The tyrosine-phosphatase PTP1B, in fact, is capable to de-phosphorylate PKM2 on Tyr-105 and Tyr-148 [22]. In the present work, to our knowledge for the first time, we suggest that also LMW-PTP acts on PKM2, de-phosphorylating this enzyme on tyrosine. The identity of the tyrosine/s involved in the mechanism remains to be elucidated.

GAPDH is tyrosine phosphorylated by Src [23] but, to our knowledge, nothing is known about the mechanism of its de-phosphorylation. On the other hand, phosphorylation of α-enolase has been associated with pancreatic cancer and leads to the production of specific auto-antibodies in pancreatic ductal adenocarcinoma patients, with diagnostic value [24]. In the case of α-enolase both kinase and phosphatase activity involved in this mechanism are not known. Finally, several evidences have demonstrated that TPIS is phosphorylated on Serine residue by Cdk2 [25], but, to our knowledge, no regulation via tyrosine phosphorylation has been yet identified. For all these three proteins, namely GAPDH, α-enolase and TPIS, our results suggest that they may be tyrosine-phosphorylated and that LMW-PTP may catalyze their tyrosine de-phosphorylation.

In addition, two other proteins, Annexin A1 and Lamin, not involved in glycolysis, has been identified by our proteomic analysis. Annexin A1 have been implicated in many cellular processes such as inflammation [26, 27, 28], glucorticoid action [29], secretion and exocytosis [30, 31, 32], cell growth and differentiation [33, 34, 35] and phosphorylated by several protein tyrosine kinase (PTKs) [36, 37]. As far as Lamin is concerned, its phosphorylation is mainly dependent on the cell cycle [38, 39, 40]. Our results indicate that both Annexin A1 and Lamin may be subjected to LMW-PTP-dependent tyrosine de-phosphorylation.

The fact that, among the six proteins selected with proteomic analysis, four of them are enzymes essential for glycolytic pathway suggests that LMW-PTP could be involved in the regulation of energetic metabolism of cancer cell. It is important to remember that, in many tumor cells and tissues, LMW-PTP is generally over-expressed with respect to normal cells [2, 4, 6, 7]. For these reasons, we decided to concentrate our attention on the LMW-PTP-dependent modulation of glucose catabolism. To evaluate short- and long-term effects of LMW-PTP inhibition, we studied metabolic profile of A375 cells treated with Morin or silenced for LMW-PTP. We previously demonstrated that the treatment with Morin causes the fast downregulation of LMW-PTP expression levels [7], while silencing deprives A375 cells of LMW-PTP for longer time. Thus, cells treated with Morin represent a model for study the acute effects of LMW-PTP inhibition, whereas silenced cells were studied to evaluate the long-term effects of LMW-PTP deprivation on energetic metabolism of cells. We found that after treatment with Morin, both glycolysis and oxygen consumption of A375 cells decrease. We speculate that this effect is in large part due to LMW-PTP

inhibition, which leads a fast PKM2 phosphorylation/inactivation. This hypothesis was confirmed by PKM2 immunoprecipitation analysis. Due to decrease of PKM2 activity, the glycolytic flow slows down, and pyruvate production falls, thereby impairing Krebs cycle, electron chain transport, oxygen consumption, and ATP production. If maintained for relatively long time, a similar metabolic asset could impair cell survival, or induce cell death. However, we clearly demonstrated that silenced cells undergo metabolic rewiring, enhancing glucose uptake and lactate production, but maintain a low oxygen consumption and producing low ROS levels respect to unsilenced cells. Moreover, we observed that silenced cells express high levels of the glucose transporter GLUT1, and hexokinase II, the first rate-limiting enzyme of glycolysis. Taken together, these results demonstrate that silenced cells acquire an evident Warburg metabolism. From a mechanistic point of view, PKM2 strongly contributes to conversion of A375 cells from a respiratory toward a glycolytic phenotype. Indeed, we found that PKM2 expression levels increased in A375 silenced cells respect to parental cells, and that silenced cells contain higher amounts of phosphorylates PKM2. Finally, we observed that LMW-PTP silencing favors migration of PKM2 dimeric form into the nucleus (see Fig.6, panel E). These evidences are in line with previous findings showing that the phosphorylated/dimeric form of PKM2 is able to migrate into the nucleus, were it acts as a transcriptional co-activator of β-catenin and hypoxia-inducible factor 1α (HIF-1α), one the master regulator of Warburg metabolism [18, 19, 41]. In synthesis, we demonstrate that in melanoma cells the overexpression of LMW-PTP is functional to maintain PKM2 in its dephosphorylate status – the tetrameric, "full active" form - which is retained in the cytoplasm, where it converts PEP in pyruvate, thereby fueling Krebs cycle and OXPHOS.

Similar effects were observed also in other cancer cells such as prostate cancer PC3, colon cancer HT29 and MEC-1 from B-cell leukemia, thereby confirming that this behavior is not a specific characteristic of the A375 melanoma cell line but, rather, represent a general feature of cancer cells expressing high LMW-PTP levels.

Considering that high LMW-PTP expression levels were found in most of aggressive cancer cells, we argue that its presence offers some advantage to cancer cells.

Based on data reported in this paper, we can exclude that high level of expression of LMW-PTP confers some vantages in term of growth rate. Rather, we observe that high level of expression of LMW-PTP enhance cell motility and invasiveness. A375, together with the other cell lines used in this work, show an aggressive phenotype, and a relative strong resistance to traditional anticancer drugs. We have already demonstrated that pharmacological inhibition of LMW-PTP increases sensitivity of melanoma, and PC3 to dacarbazine, 5-FU and radiotherapy [7]. Similar results were reported by others, in a study conducted on colon cancer cells [6]. Together, these evidences

suggest that LMW-PTP could be involved in the acquisition of an aggressive phenotype, rather than stimulate growth rate of cancer cells. The exact mechanism that link LMW-PTP expression, PKM2 activation and resistance to apoptosis remains to be clarified.

4.1. Conclusions

In this work we can clearly assess that high LMW-PTP expression, which is common in tumor cells, negatively influences the rate of glycolysis. This regulation is very probably due to the fact that LMW-PTP modulate the tyrosine phosphorylation level of at least four different enzymes involved in glycolysis. Moreover, we show that changes in expression levels of LMW-PTP leads to the control of invasiveness and cell proliferation rate.

Much more work is needed to precisely understand the consequences of tyrosine phosphorylation control at the level of the proteins that we have identified as new LMW-PTP substrates.

Funding

Istituto Toscano Tumori (Messori-ITT-2015)

Fondi di Ateneo-University of Florence – Italy

PP acknowledges AIRC (Associazione Italiana per la Ricerca sul cancro) for the project "Assaying tumor metabolic deregulation in live cells"; project code 19515.

Conflict of interest

The authors have no conflicts of interest to declare.

5. References

[1] P. Chiarugi, M.L. Taddei, N. Schiavone, L. Papucci, E. Giannoni, T. Fiaschi, S. Capaccioli, G. Raugei, G. Ramponi, LMW-PTP is a positive regulator of tumor onset and growth, Oncogene, 23 (2004) 3905-14.

[2] F. Malentacchi , R. Marzocchini , S. Gelmini , C. Orlando , M. Serio , G. Ramponi , G. Raugei , Up-regulated expression of low molecular weight protein tyrosine phosphatases in different human cancers, Biochem Biophys Res Commun. 334 (2005) 875-83.

[3] R. Marzocchini, F. Malentacchi, M. Biagini, D. Cirelli, C. Luceri, G. Caderni, G. Raugei, The expression of low molecular weight protein tyrosine phosphatase is up-regulated in 1,2-dimethylhydrazine-induced colon tumours in rats, Int J Cancer. 122 (2008) 1675-8.

[4] R.R. Ruela-de-Sousa, E. Hoekstra, A.M. Hoogland, K.C. Queiroz, M.P. Peppelenbosch, A.P. Stubbs, K . Pelizzaro-Rocha, G.J. van Leenders, G. Jenster, H. Aoyama, C.V. Ferreira, G.M. Fuhler, Low-Molecular-Weight Protein Tyrosine Phosphatase Predicts Prostate Cancer Outcome by Increasing the Metastatic Potential, Eur Urol. 69 (2016) 710-9.

[5] P.A. Ferreira, R.R. Ruela-de-Sousa, K.C. Queiroz, A.C. Souza, R. Milani, R.A. Pilli, M.P. Peppelenbosch, J. den Hertog, C.V. Ferreira, Knocking down low molecular weight protein tyrosine phosphatase (LMW-PTP) reverts chemoresistance through inactivation of Src and Bcr-Abl proteins, PLoS One, 7 (2012) 44312.

[6] E. Hoekstra, L.L. Kodach, A.M. Das, R.R. Ruela-de-Sousa, C.V. Ferreira, J.C. Hardwick, C.J. van der Woude, M.P. Peppelenbosch, T.L. Ten Hagen, G.M. Fuhler, Low molecular weight protein tyrosine phosphatase (LMWPTP) upregulation mediates malignant potential in colorectal cancer, Oncotarget 6 (2015) 8300-12.

[7] G. Lori, P. Paoli, A. Caselli, P Cirri, R Marzocchini, M. Mangoni, C. Talamonti, L. Livi, G Raugei, Targeting LMW-PTP to sensitize melanoma cancer cells toward chemo- and radiotherapy, Cancer Medicine, (2018) doi: 10.1002/cam4.1435

[8] P. Chiarugi, P Cirri, F Marra F, G Raugei, G Camici, G Manao, G Ramponi G, LMW-PTP is a negative regulator of insulin-mediated mitotic and metabolic signaling, Biochem Biophys Res Commun. 1997 238 (1997) 676-82.

[9] S.M. Stanford, A.E. Aleshin, V. Zhang, R.J. Ardecky, M.P. Hedrick, J. Zou, S.R. Ganji, M.R. Bliss, F. Yamamoto, A.A. Bobkov, J. Kiselar, Y. Liu, G.W. Cadwell, S. Khare, J. Yu, A. Barquilla, T.D.Y. Chung, T. Mustelin, S. Schenk, L.A. Bankston, R.C. Liddington, A.B. Pinkerton, N. Bottini, Diabetes reversal by inhibition of the low-molecular-weight tyrosine phosphatase, Nat Chem Biol. 13 (2017) 624-632.

[10] A.V. Faria, T.F. Tornatore, R. Milani, K.C.S. Queiroz, I.H. Sampaio, E.M.B. Fonseca, K.J.P. Rocha-Brito, T.O. Santos, L.R. Silveira, M.P. Peppelenbosch, C.V. Ferreira-Halder, Oncophosphosignaling Favors a Glycolytic Phenotype in Human Drug Resistant Leukemia, J Cell Biochem. 118 (2017) 3846-3854.

[11] A. Caselli, P. Paoli, A. Santi, C. Mugnaioni, A. Toti, G. Camici, P. Cirri, Low molecular weight protein tyrosine phosphatase: Multifaceted functions of an evolutionarily conserved enzyme, Biochim Biophys Acta 1864 (2016) 1339-55.

[12] P. Chiarugi, P. Cirri, G. Raugei, G. Camici, F. Dolfi, A. Berti, G. Ramponi, PDGF receptor as a specific in vivo target for low M(r) phosphotyrosine protein phosphatase, FEBS Lett. 372 (1995) 49-53.

[13] A. Carpentieri, T. Gamberi, A. Modesti, A. Amoresano, B. Colombini, M. Nocella, M.A. Bagni, T. Fiaschi, L. Barolo, M. Gulisano, F. Magherini, Profiling Carbonylated Proteins in Heart and Skeletal Muscle Mitochondria from Trained and Untrained Mice, J Proteome Res. 15 (2016) 3666-3678.

[14] T. Gamberi , T. Fiaschi, E. Valocchia, A. Modesti, P. Mantuano, J.F. Rolland, F. Sanarica, A. De Luca, F. Magherini, Proteome analysis in dystrophic mdx mouse muscle reveals a drastic alteration of key metabolic and contractile proteins after chronic exercise and the potential modulation by anti-oxidant compounds, J Proteomics, 170 (2018) 43-58.

[15] W. Yanga, Z. Lua, Regulation and function of pyruvate kinase M2 in cancer, Cancer Lett. 339 (2013) 153–158.

[16] D. Anastasiou, Y. Yu, W.J. Israelsen, J.K. Jiang, M.B. Boxer, B.S. Hong BS, W. Tempel, S. Dimov, M. Shen, A. Jha, H. Yang, K.R. Mattaini, C.M. Metallo, B.P. Fiske, K.D. Courtney, S. Malstrom, T.M. Khan, C. Kung, A.P. Skoumbourdis, H. Veith, N. Southall, M.J. Walsh, K.R. Brimacombe, W. Leister, S.Y. Lunt, Z.R. Johnson, K.E. Yen, K. Kunii, S.M. Davidson, H.R. Christofk, C.P. Austin, J. Inglese, M.H. Harris, J.M. Asara, G. Stephanopoulos, F.G. Salituro, S. Jin, L. Dang, D.S. Auld, H.W. Park, L.C. Cantley, C.J. Thomas, M.G. Vander Heiden, Pyruvate kinase M2 activators promote tetramer formation and suppress tumorigenesis, Nat Chem Biol. 8 (2012) 839–847.

[17] X. Gao, H. Wang, J.J. Yang, X. Liu, Z.R. Liu, Pyruvate kinase M2 regulates gene transcription by acting as a protein kinase, Mol Cell. 45 (2012) 598–609.

[18] W. Luo, H. Hu, R. Chang, J. Zhong, M. Knabel, R. O'Meally, R.N. Cole, A. Pandey, G.L. Semenza, Pyruvate kinase M2 is a PHD3-stimulated coactivator for hypoxia-inducible factor 1"; Cell.; (2011); 145:732–744.

[19] W. Yang, Y. Xia, H. Ji, Y. Zheng, J. Liang, W. Huang, X. Gao, K. Aldape, Z. Lu, Nuclear PKM2 regulates beta-catenin transactivation upon EGFR activation, Nature, 480 (2011) 118–122.

[20] I. Samudio, M. Fiegl, M. Andreeff, Mitochondrial uncoupling and the Warburg effect: molecular basis for the reprogramming of cancer cell metabolism, Cancer Res. 69 (2009) 2163–6.

[21] W.H. Koppenol, P.L. Bounds, C.V. Dang, Otto Warburg's Contributions to current concepts of cancer metabolism, Nat. Rev. Cancer. 2011; 11 (2011) 325–37.

[22] A. Bettaieb, J. Bakke, N. Nagata, K. Matsuo, Y. Xi, S. Liu, D. AbouBechara, R. Melhem, K. Stanhope, B. Cummings, J. Graham, A. Bremer, S. Zhang, C.A. Lyssiotis, Z.Y. Zhang, L.C. Cantley, P.J. Havel, F.G. Haj, Protein tyrosine phosphatase 1B regulates pyruvate kinase M2 tyrosine phosphorylation, J Biol Chem. 288 (2013) 17360-71.

[23] E.J. Tisdale, C.R. Artalejo, A GAPDH Mutant Defective in Src-Dependent Tyrosine Phosphorylation Impedes Rab2-Mediated Events, Traffic, 8 (2007) 733–741.

[24] B. Tomaino, P. Cappello, M. Capello, C. Fredolini, I. Sperduti, P. Migliorini, P. Salacone, A. Novarino , A. Giacobino, L. Ciuffreda, M. Alessio, P. Nisticò, A. Scarpa, P. Pederzoli, W. Zhou, E.F. Petricoin Iii, L.A. Liotta, M. Giovarelli, M. Milella, F. Novelli, Circulating autoantibodies to phosphorylated α-enolase are a hallmark of pancreatic cancer, Journal of Proteome Research, 10 (2011) 105–112.

[25] W.H. Lee, J.S. Choi, M.R. Byun, K.T. Koo, S. Shin, S.K. Lee, Y.J. Surh, Functional inactivation of triosephosphate isomerase through phosphorylation during etoposide-induced apoptosis in HeLa cells: potential role of Cdk2, Toxicology, 278 (2010) 224-8.

[26] G. Cirino, R.J. Flower, Human recombinant lipocortin I inhibits prostacyclin production by human umbilical artery in vitro, Prostaglandins, 34 (1987) 59-62.

[27] M. Perretti, Lipocortin I and chemokine modulation of granulocyte and monocyte accumulation in experimental inflammation, Gen. Pharmacol. 31 (1998) 545-552.

[28] F. Carey, R. Forder, M.D. Edge, A.R. Greene, M.A. Horan, P.J. Strijbos, N.J. Rothwell, Lipocortin I fragment modifies pyrogenic actions of cytokines in rats, Am. J. Physiol. 259 (1990) 266-269.

[29] W.T. Wong, S.C. Frost, H.S. Nick, Protein-synthesis-dependent induction of annexin I by glucocorticoid, Biochem. J. 275 (1992) 313-319.

[30] R.D. Burgoyne, Calpactin in exocytosis, Nature, 331 (1988) 20.

[31] M. Ohnishi, M. Tokuda, T. Masaki, T. Fujimura, Y. Tai, T. Itano, H Matsui, T. Ishida, R, Konishi, J. Takahara, O. Hatase, Involvement of Annexin I in glucose-induced insulin secretion in rat pancreatic islets, Endocrinology, 136 (1995) 2421-2426.

[32] J.C. Buckingham, R.J. Flower, Lipocortin I: A second messenger of glucocorticoid action in the hypothalamo-pituitary-adrenocortical axis, Mol. Med. Today 3 (1997) 296-302.

[33] J.F. Tait, M. Sakata, B.A. McMullen, C.H. Miao, T. Funakoshi, L.E. Hendrickson, K. Fujikawa, Placental anticoagulant proteins: Isolation and comparative characterization four members of the lipocortin family, Biochemstry, 27 (1988) 6268-6276.

[34] F. William, B. Mroczkowski, S. Cohen, A.S. Kraft, Differentiation of HL-60 cells is associated with an increase in the 35-kDa protein lipocortin I, J. Cell. Physiol. 137 (1988) 402-410.

[35] M.T. Fox, D.A. Prentice, J.P. Hughes, Increase in p11 and annexin II proteins correlate with differentiation in the PC12 pheochromocytoma, Biochem. Biophys. Res. Commun. 177 (1991) 1188-1193.

[36] E. Erikson, R.L. Erikson, Identification of a cellular protein substrate phosphorylated by the avian sarcoma virus-transforming gene product, Cell 21 (1980) 829-836.

[37] R.A. Fava, S. Cohen, Isolation of a calcium-dependent 35-kilodalton substrate for the epidermal growth factor receptor/kinase from A-431 cells, J. Biol. Chem. 259 (1984) 2636-2645.

[38] B. Lüscher, L. Brizuela, D. Beach, R.N. Eisenman, A role for the p34cdc2 kinase and phosphatases in the regulation of phosphorylation and disassembly of lamin B2 during the cell cycle, EMBO J 1991.

[39] Y. Ottaviano, L. Gerace, Phosphorylation of the nuclear lamins during interphase and mitosis, J. Biol. Chem. 260 (1985) 624-32.

[40] R. Rzepecki, P.A. Fisher, In vivo phosphorylation of drosophila melanogaster nuclear lamins during both interphase and mitosis, Cell. Mol. Biol. Lett. 7 (2002) 859-76.

[41] E. Giannoni, M.L. Taddei, a. Morandi, G. Comit, M. Calvani, F. Bianchini, B. Richichi, G. Raugei, N. Wong, D. Tang, P. Chiarugi, Targeting stromal-induced pyruvate kinase M2 nuclear translocation impairs oxphos and prostate cancer metastatic spread, Oncotarget, 6 (2015) 24061-74.

Figure captions

Fig.1 A375 human melanoma cells silenced for LMW-PTP. Transfection time course: A375 cells were silenced with siRNA or scramble (20nM). Western blots were conducted at 18 h, 28 h and 36 h after transfection. In panel A, a representative experiment is shown. In panel B, a densitometric analysis is presented as result of three independent experiments.

Fig.2 Representative 2-D phospho-blots and Colloidal Coomassie stained gels of cells silenced for LMW-PTP cells and of control cells. Sample proteins from control (**A**) and LMW-PTP-silenced cells (**B**) were separated by IEF (11 cm, 3–10 NL). Second dimension was performed in 9–16% polyacrylamide linear gradient and phosphorylated proteins were detected by western blot. In panel, (**C**) and (**D**) the corresponding colloidal Coomassie stained gels are shown. For each cell specimen (LMW-PTP-silenced cells and control cells), six colloidal Coomassie-stained gels and six 2-D phospho-blots were performed. Statistical analysis was carried out by ImageMaster 2D Platinum software v7.0 (GE Healthcare) using a two-tailed Student's t-test. Circles and numbers indicate the statistical differentially phosphorylated spots ($p<0.05$) identified by MS.

Fig.3 Validation of novel substrates of LMW-PTP using immuno and co-immunoprecipitation. (**A-F**) Immunoprecipitation analysis of α-Enolase, PKM2, GAPDH, TPIS, Annexin A1 and Lamin A/C using appropriate antibodies. Samples were subjected to SDS-PAGE and analyzed by Western Blotting using 4G10 anti-pTyr antibodies. For each co-immunoprecipitation, western blot with the antibodies for PKMM1, ENO1, GAPDH, TPIS, Annexin 1 and prelamin-A/C was performed. In the histograms the quantification is shown, as phosphorylated form of the protein/ total protein. (**G**) Co-immunoprecipitation analysis of PKM2, αEnolase, GAPDH, TPIS, Annexin A1 and Lamin A/C using anti-LMW-PTP antibody. DU145 cells mock-transfected or transfected with the *Dn* form of LMW-PTP were used. Co-immunoprecipitation control with an irrelevant antibody (GM130, Santa Cruz Biotechnology SC-16268) gave negative results (data not shown).

Fig.4 Energetic profile of A375 cells treated with Morin. Cells were starved for 16 hours and then incubated for further 4 hours at 37°C in the presence of starvation medium containing (open circles), or not (black circles), 50 µM Morin. After, cells were washed with PBS and then analysed by using Seahorse technology (Agilent Technologies Inc., US). (**A**), oxygen consumption rate; (**B**), extracellular acidification rate; (**C**), OCR/ECAR ratio in basal condition; (**D**), maximal respiration determined after treatment of A375 cells with FCCP. Data reported in the figure represent the mean

values ± S.D. (n = 8) ** p < 0.05; *** p < 0.001; (**E-F**) Immunoprecipitation analysis of PKM2 phosphorylation levels after treatment with Morin. PKM2 was immunoprecipitated and analysed by SDS-PAGE separation and western blot. Equivalent amount of total protein was leaded on gels. Phosphorylation status on tyrosine residue of PKM2 was detected by using monoclonal 4G10 anti-phosphotyrosine antibodies (Millipore). The experiment was carried out in duplicate. (**E**) representative western blot analysis; (**F**) Images were acquired by using Amersham Imager 600 luminometer (Amersham). Quantification of bands was carried out by using the Amersham quantification software. Data reported in the figure represent the mean value ± S.E.M. (n = 2).

Fig.5 LMW-PTP silencing induces metabolic switch in A375 human melanoma cells. All the experiments were performed on A375 cells, 28 h after transfection. (**A**) Glucose uptake. Cells were incubated with (U-^{14}C) deoxy-D-Glucose and then lysed with 0.1M NaOH. The amount of up-taken glucose was measured using a scintillator analyzer. (**B**) Lactate production. The medium of silenced and control cells was collected, and lactate amount was measured using a commercial kit. (**C**) Oxygen consumption. The rate of O_2 consumption was evaluated using a Clark-type O_2 electrode from Hansatech. Values obtained for three independent experiments were normalized on cells number. (**D**) ROS level. Intracellular ROS level were measured using ROS detection assay (DCFDA).

Fig.6 LMW-PTP is involved in the regulation of key-glycolytic enzymes: A375 cells were transfected with siRNA or scramble. (**A**) After 24h cells were lysed and analyzed by western blot with specific primary antibody against PKM2, GLUT1 and HKII. (**B**, **C**, **D**) Densitometric analysis were obtained using actin as internal control. (**E**) Melanoma transfected cells were subjected to nuclear extraction, as described in Methods, to measure the amount of cytosolic and nuclear form of PKM2. To assess the grade of this purification, actin content, in both compartment, was evaluated.

Fig.7 LMW-PTP affects cell growth and invasiveness of A375 melanoma cells. (**A**) A375 cells were transfected with siRNA or scramble. After 24, 48 and 72h cells were detached and counted with a Burker chamber, using contrast phase microscope. The invasive ability of Melanoma silenced cells was determined using Boyden chamber assay (**B**) and measuring MMP2 activity in a gel zimography (**C**). After 28h of scramble or siRNA transfection, total RNA was extracted, and mRNA levels of LMW-PTP, SLUG, SNAIL and E-cadherin were determined with RT-PCR (**D-G**).

Fig.S1 LMW-PTP regulates metabolism of PC3 prostate cancer cells. (**A**) PC3 cells, 28h after siRNA or scramble transfection, were lysed and analysed by western blotting to validate LMW-PTP silencing. Actin was used as internal control for densitometric analysis. (**B**) Glucose uptake. PC3 cells were incubated with (U-14C) deoxy-D-Glucose for 30 minutes, then washed twice with cold PBS and lysed with 0.1M NaOH. The amount of radioactive up-taken glucose from the cells was measured using a scintillator analyzer. All values were normalized to protein content. (**C**) Lactate production. The medium of silenced and control cells was collected, and lactate amount was measured using a commercial kit. L-Lactate content was normalized to protein content. (**D**) Oxygen consumption, 28h after silencing, were carried using a Clark-type O_2 electrode from Hansatech.

Fig.S2 LMW-PTP regulates metabolism of HT29 colon cancer cells: The experiments were performed on the HT29 colon cancer cell line, as described in Fig. S1. (**A**) validation of LMW-PTP silencing by western blot. (**B**) Glucose uptake. (**C**) Lactate production. (**D**) Oxygen consumption, 28h after silencing, were carried using a Clark-type O_2 electrode from Hansatech.

Fig.S3 LMW-PTP regulates metabolism of MEC-1 chronic B leukemia cells. The experiments were performed on the MEC-1 colon cancer cell line, as described in Fig. S1. (**A**) validation of LMW-PTP silencing by western blot. (**B**) Glucose uptake. (**C**) Lactate production. (**D**) Oxygen consumption, 28h after silencing, were carried using a Clark-type O_2 electrode from Hansatech.

Table 1: Differentially tyrosine-phosphorylated proteins identified by MALDI-TOF mass spectrometry.

Spot n.[a]	Protein	AC[b]	Gene	GO Biological Process[c]	Mascot search results			p-value[g]	Fold change siRNA vs control[h]
					Score[d]	Matched Pept.[e]	Seq. coverage (%)[f]		
1	Prelamin-A/C	P02545	LMNA	Establishment or maintenance of microtubule cytoskeleton polarity GO:003095	96	14/50	22	0.0066	1.5
2	Prelamin-A/C	P02545	LMNA	Establishment or maintenance of microtubule cytoskeleton polarity GO:003095	130	18/34	27	0.005	1.5
3	Prelamin-A/C	P02545	LMNA	Establishment or maintenance of microtubule cytoskeleton polarity GO:003095	155	22/47	31	0.001	3.2
4	Alpha-enolase	P06733	ENO1	Canonical glycolysis GO:0061621	158	18/43	24	0.0009	2.2
5	Pyruvate kinase	P14618	PKM	Canonical glycolysis GO:0061621	204	30/83	61	<0.0001	2.8
6	Annexin A1	P04083	ANXA1	Cell-cell adhesion GO:0098609 Negative	137	13/38	42	0.0009	2.9

				regulation of apoptotic process GO:0043066					
7	Glyceraldehyde-3-phosphate dehydrogenase	P04406	GAPDH	Canonical glycolysis GO:0061621	178	16/45	29	0.0003	1.8
8	Triosephosphate isomerase	P60174	TPIS	Canonical glycolysis GO:0061621	110	14/40	38	<0.0001	2

[a] Spot numbers match those reported in the representative 2-DE images shown in Fig.2.
[b] Accession number in Swiss-Prot/UniprotKB (www.uniprot.org/).
[c] Functional categories based on the Gene Ontology (GO) terms related to their major biological process using Nextprot database (https://www.nextprot.org/), data release 2017-08-01 Application release v2.10.0.
[d] MASCOT MS score (Matrix Science, London, UK; http://www.matrixscience.com). MS matching score greater than 56 was required for a significant MS hit (p-value<0.05).
[e] Number of matched peptides corresponds to peptide masses matching the top hit from Ms-Fit PMF, searched peptide are also reported.
[f] Sequence coverage = (number of the identified residues/total number of amino acid residues in the protein sequence) x100%.
[g] The p-value listed is the significance of altered phosphorylation levels relative to control samples with $p < 0.05$.
[h] Fold change (siRNA PTP vs control) was calculated dividing the phosphorylation index (see methods for details) of siRNA PTP cells with that of control cells.

Table 2: Primer sequence utilized for RT-PCR.

GENE	FORWARD (5' to 3')	REVERSE (3' to 5')
LMW-PTP	GGAAACTTGTAACCGATCAAAACA	CCCACGTTCCAGTCAGAAACA
SNAIL	GCTGCAGGACTCTAATCCAGAGTT	GACAGAGTCCCAGATGAGCATTG
SLUG	AGATGCATATTCGGACCCAC	CCTCATGTTTGTGCAGGAGA
E-Cadherin	CAGCCCAAAGTGTGTGAGAA	TGTGATGTTGGCCGTGTTAT
GAPDH	GGACCTGACCTGCCGTCTAGAA	GGTGTCGCTGTTGAAGTCAGAG

Figure 1

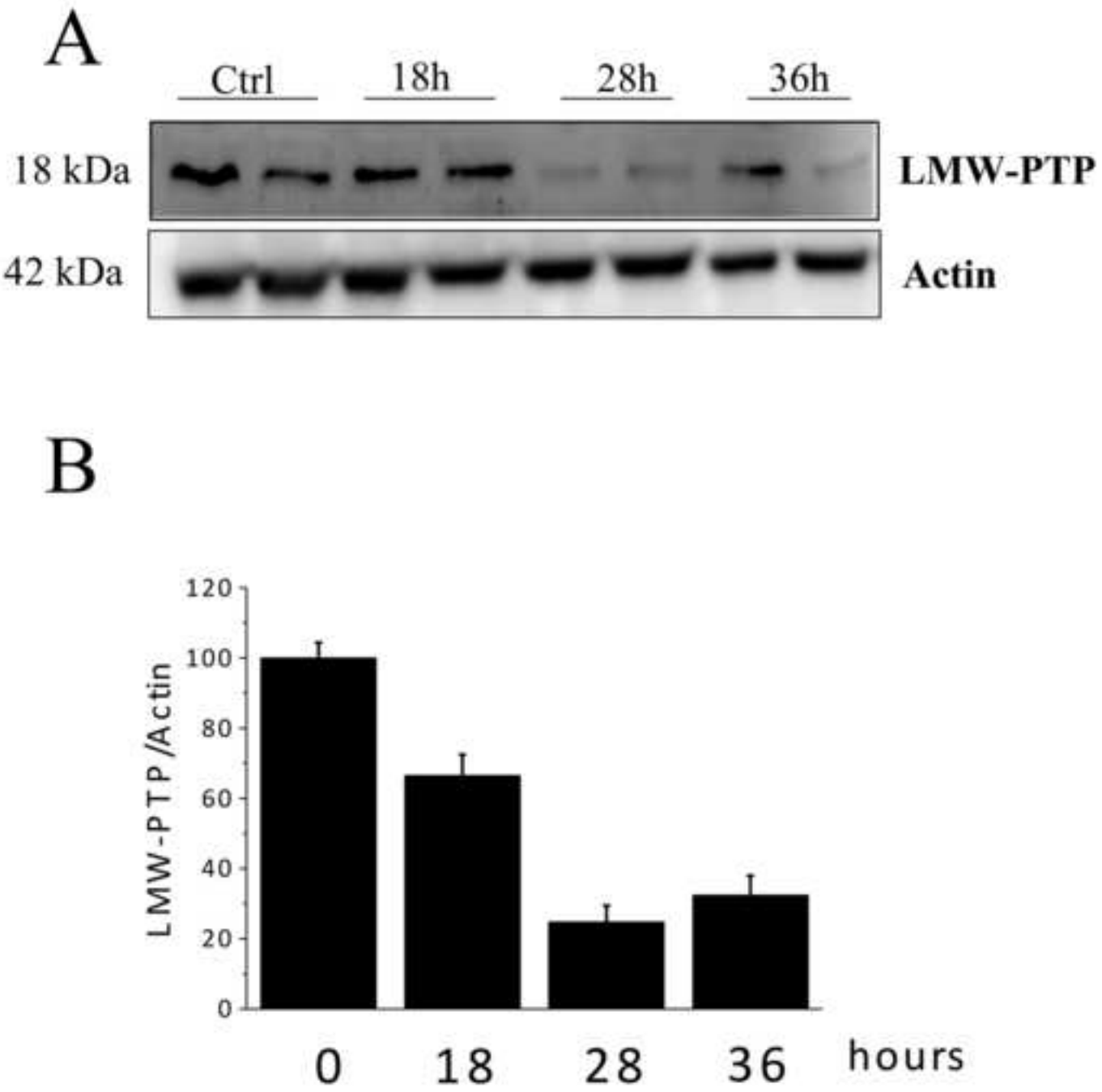
A
Ctrl
18h
28h
36h
18 kDa
LMW-PTP
42 kDa
Actin
B
LMW-PTP/Actin
120
100
80
60
40
20
0
0
18
28
36
hours

Figure 2

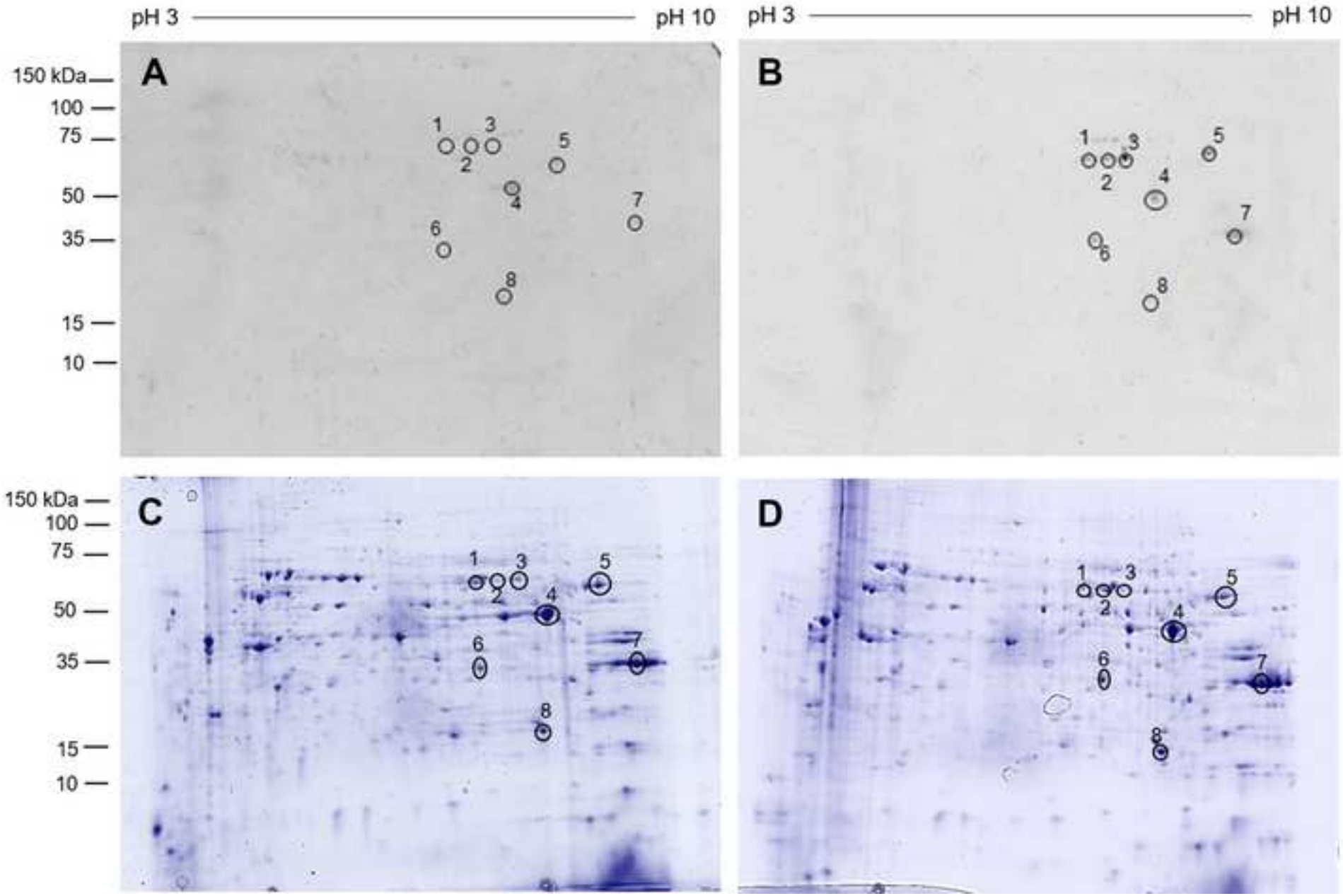

Figure 3

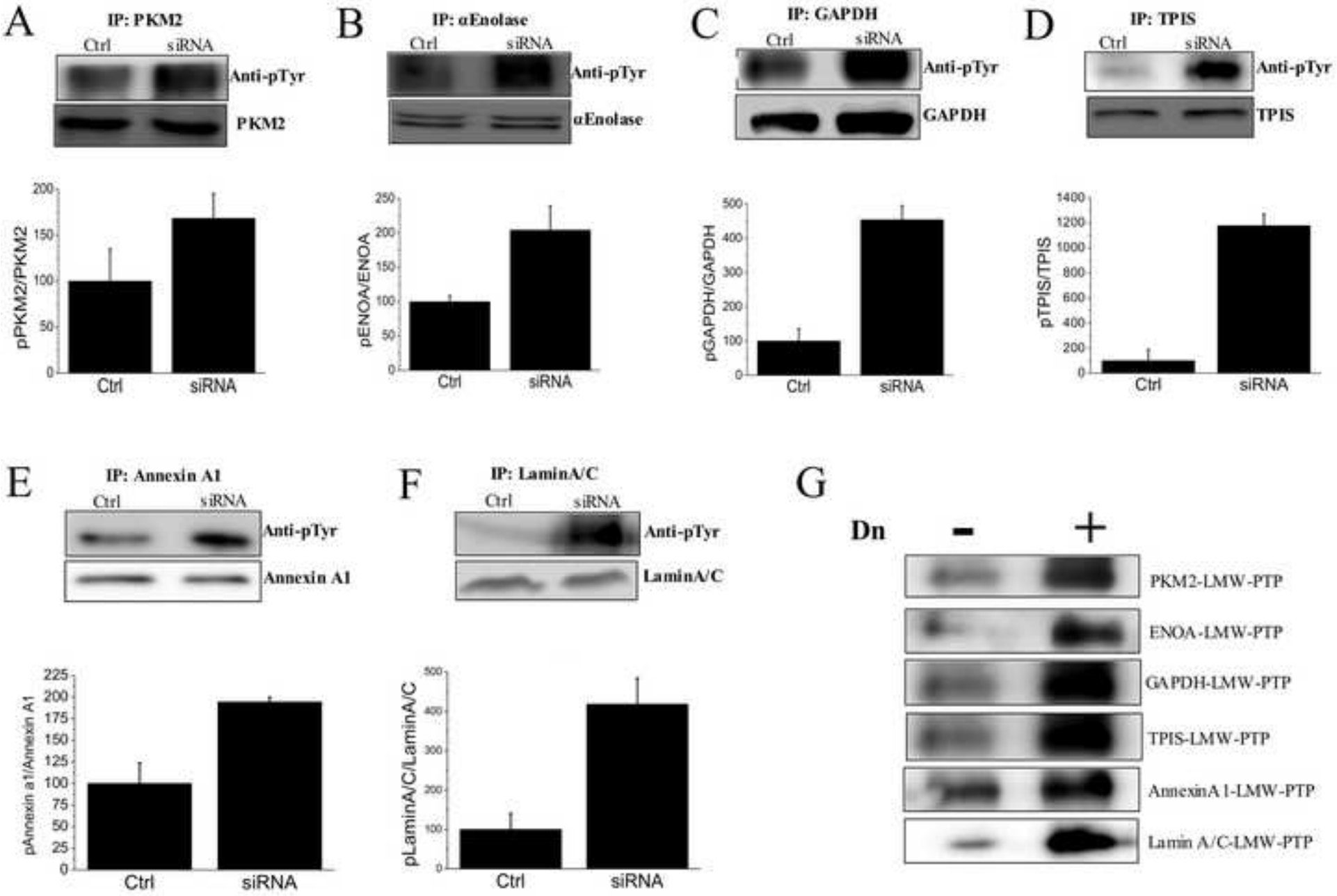
A
IP: PKM2
Ctrl
siRNA
Anti-pTyr
PKM2
pPKM2/PKM2
Ctrl
siRNA
B
IP: αEnolase
Ctrl
siRNA
Anti-pTyr
αEnolase
pENOA/ENOA
Ctrl
siRNA
C
IP: GAPDH
Ctrl
siRNA
Anti-pTyr
GAPDH
pGAPDH/GAPDH
Ctrl
siRNA
D
IP: TPIS
Ctrl
siRNA
Anti-pTyr
TPIS
pTPIS/TPIS
Ctrl
siRNA
E
IP: Annexin A1
Ctrl
siRNA
Anti-pTyr
Annexin A1
pAnnexin a1/Annexin A1
Ctrl
siRNA
F
IP: LaminA/C
Ctrl
siRNA
Anti-pTyr
LaminA/C
pLaminA/C/LaminA/C
Ctrl
siRNA
G
Dn
-
+
PKM2-LMW-PTP
ENOA-LMW-PTP
GAPDH-LMW-PTP
TPIS-LMW-PTP
AnnexinA1-LMW-PTP
Lamin A/C-LMW-PTP

Figure 4

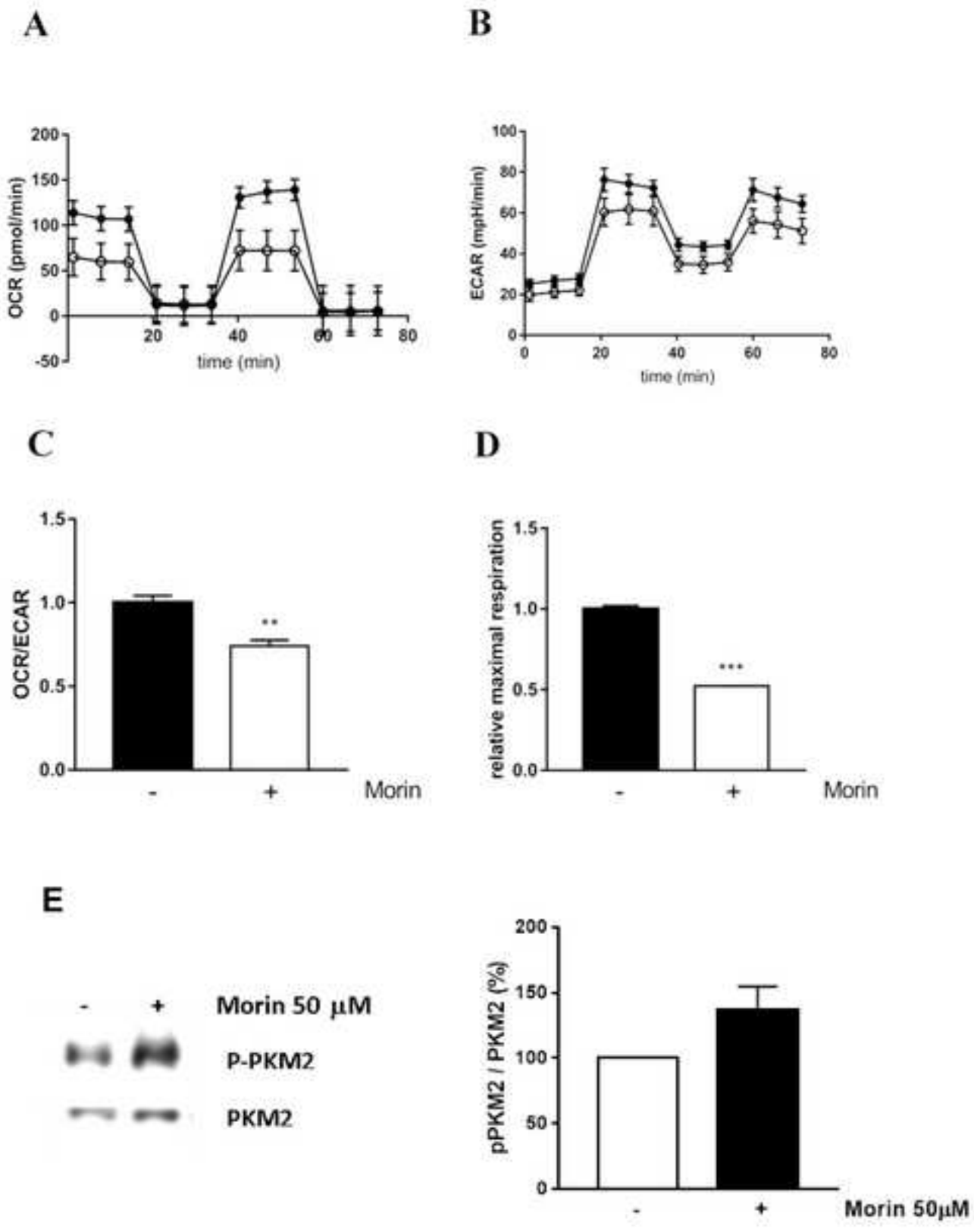
A
OCR (pmol/min)
time (min)
B
ECAR (mpH/min)
time (min)
C
OCR/ECAR
**
Morin
D
relative maximal respiration
***
Morin
E
Morin 50 μM
P-PKM2
PKM2
pPKM2 / PKM2 (%)
Morin 50μM

Figure 5

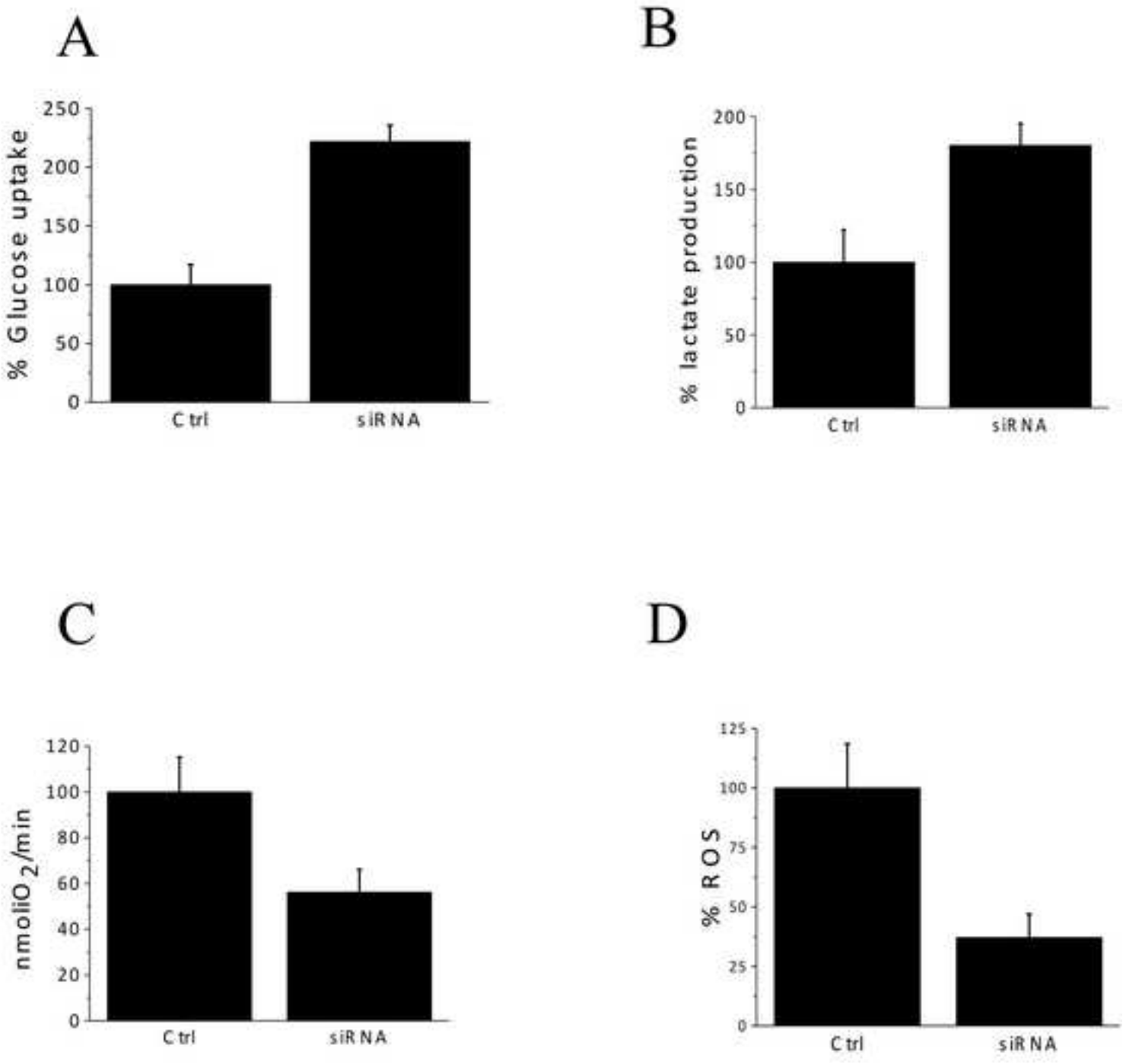
A
% Glucose uptake
250
200
150
100
50
0
Ctrl
siRNA
B
% lactate production
200
150
100
50
0
Ctrl
siRNA
C
nmoliO2/min
120
100
80
60
40
20
0
Ctrl
siRNA
D
% ROS
125
100
75
50
25
0
Ctrl
siRNA

Figure 6

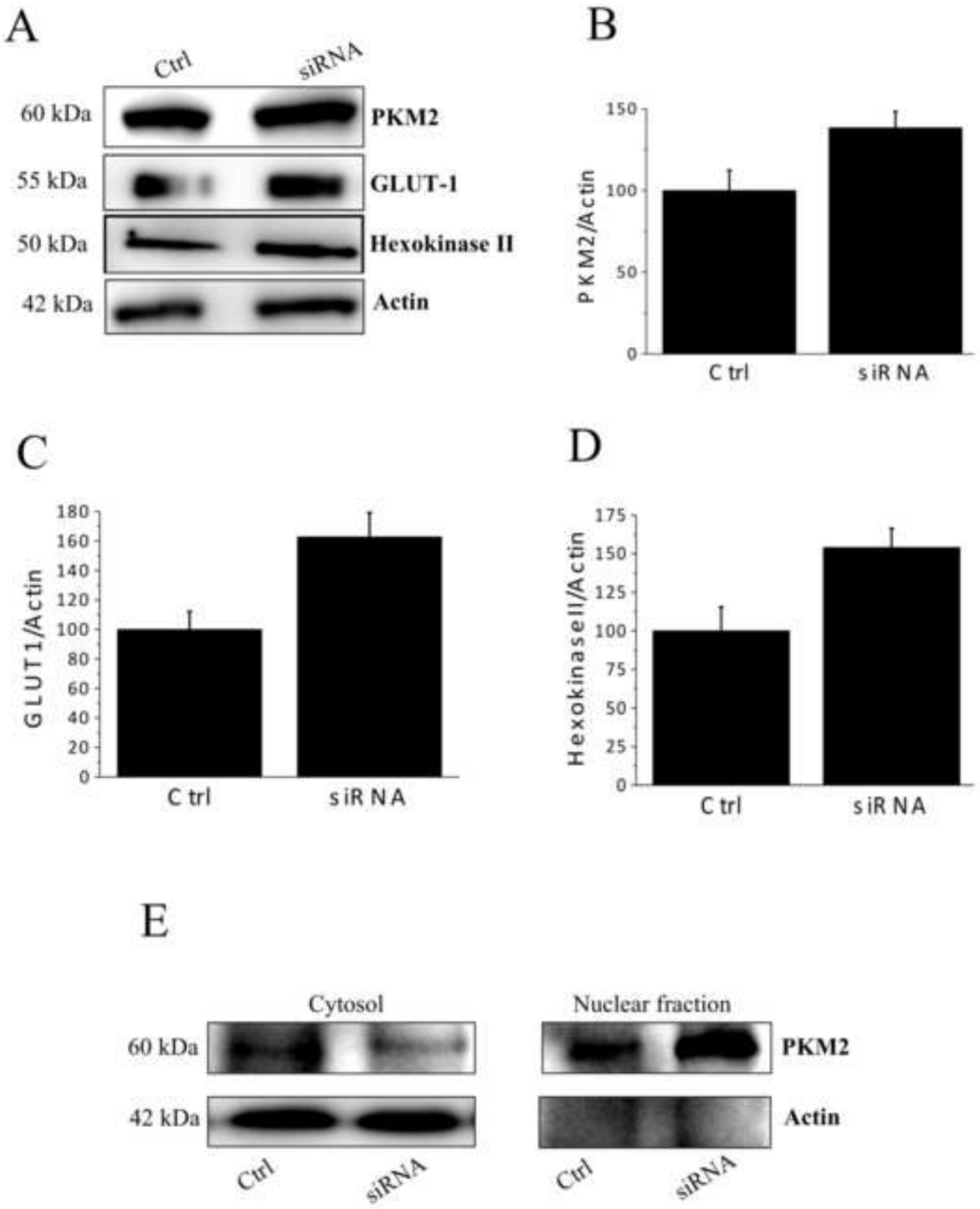
A
Ctrl
siRNA
60 kDa
PKM2
55 kDa
GLUT-1
50 kDa
Hexokinase II
42 kDa
Actin
B
PKM2/Actin
150
100
50
0
Ctrl
siRNA
C
GLUT1/Actin
180
160
140
120
100
80
60
40
20
0
Ctrl
siRNA
D
HexokinaseII/Actin
175
150
125
100
75
50
25
0
Ctrl
siRNA
E
Cytosol
Nuclear fraction
60 kDa
PKM2
42 kDa
Actin
Ctrl
siRNA
Ctrl
siRNA

Figure 7

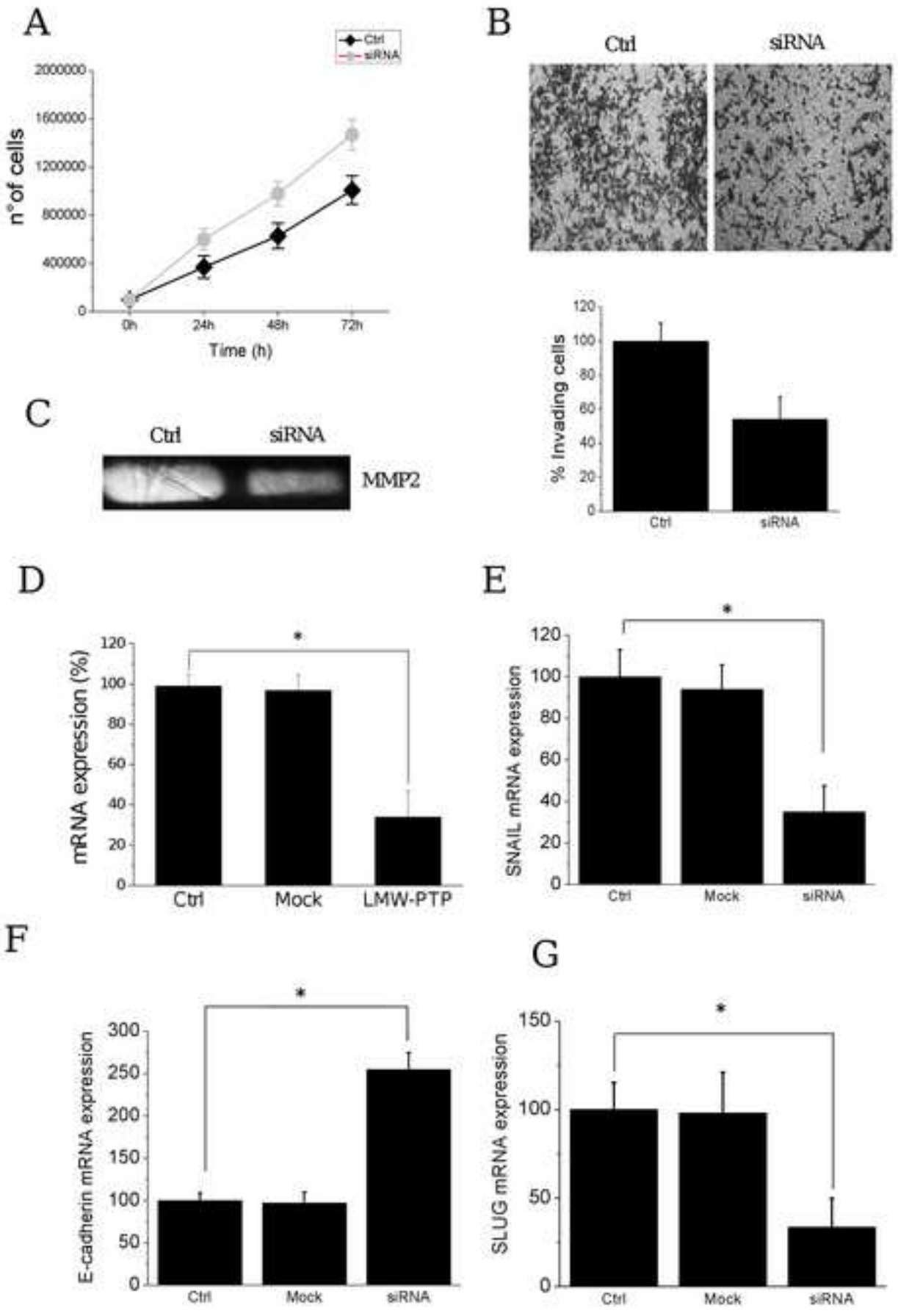
A
Ctrl
siRNA
n°of cells
2000000
1600000
1200000
800000
400000
0
0h
24h
48h
72h
Time (h)
B
Ctrl
siRNA
% Invading cells
120
100
80
60
40
20
0
Ctrl
siRNA
C
Ctrl
siRNA
MMP2
D
mRNA expression (%)
120
100
80
60
40
20
0
*
Ctrl
Mock
LMW-PTP
E
SNAIL mRNA expression
120
100
80
60
40
20
0
*
Ctrl
Mock
siRNA
F
E-cadherin mRNA expression
300
250
200
150
100
50
0
*
Ctrl
Mock
siRNA
G
SLUG mRNA expression
150
100
50
0
*
Ctrl
Mock
siRNA

Figure S1

Click here to download high resolution image

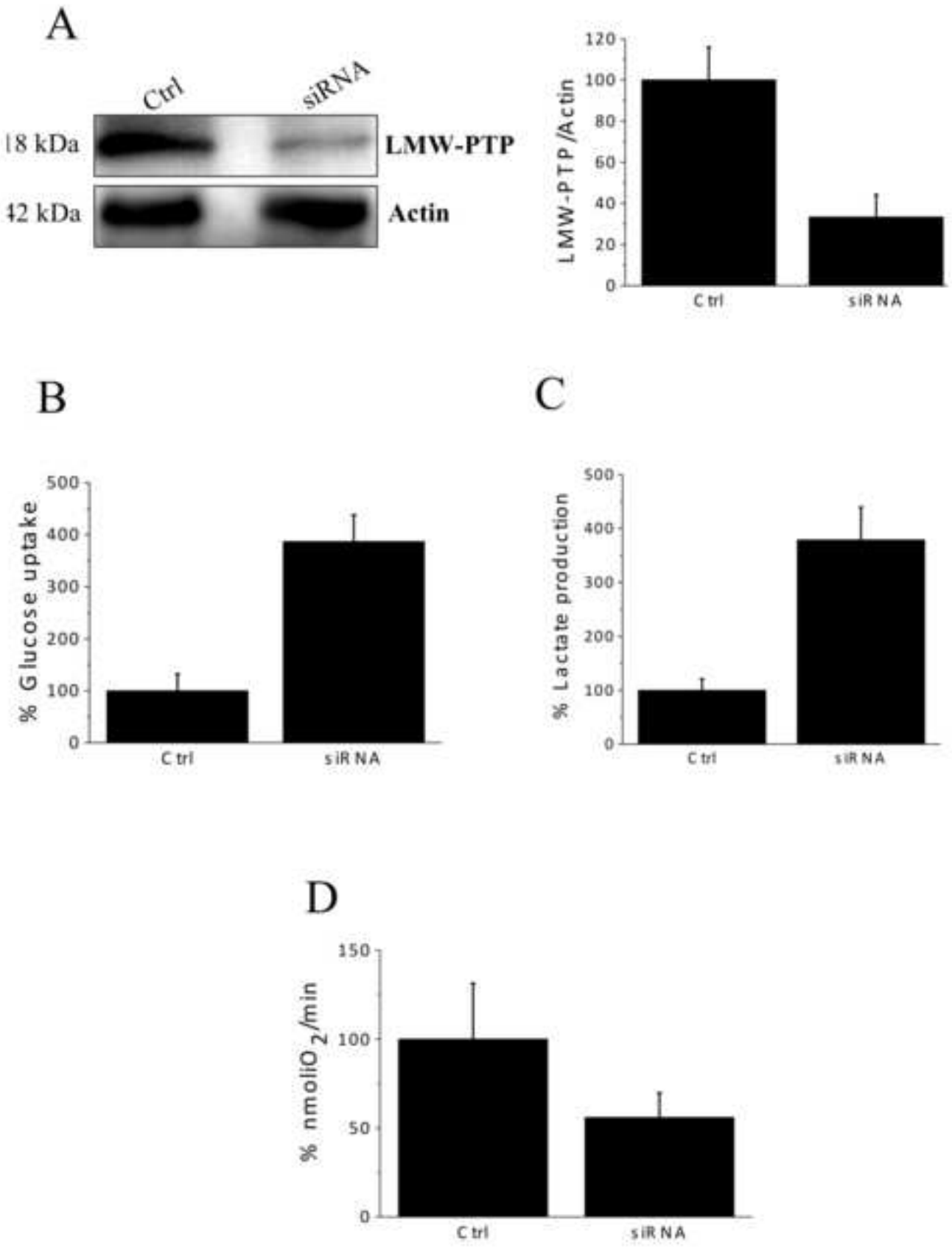

Figure S2

Click here to download high resolution image

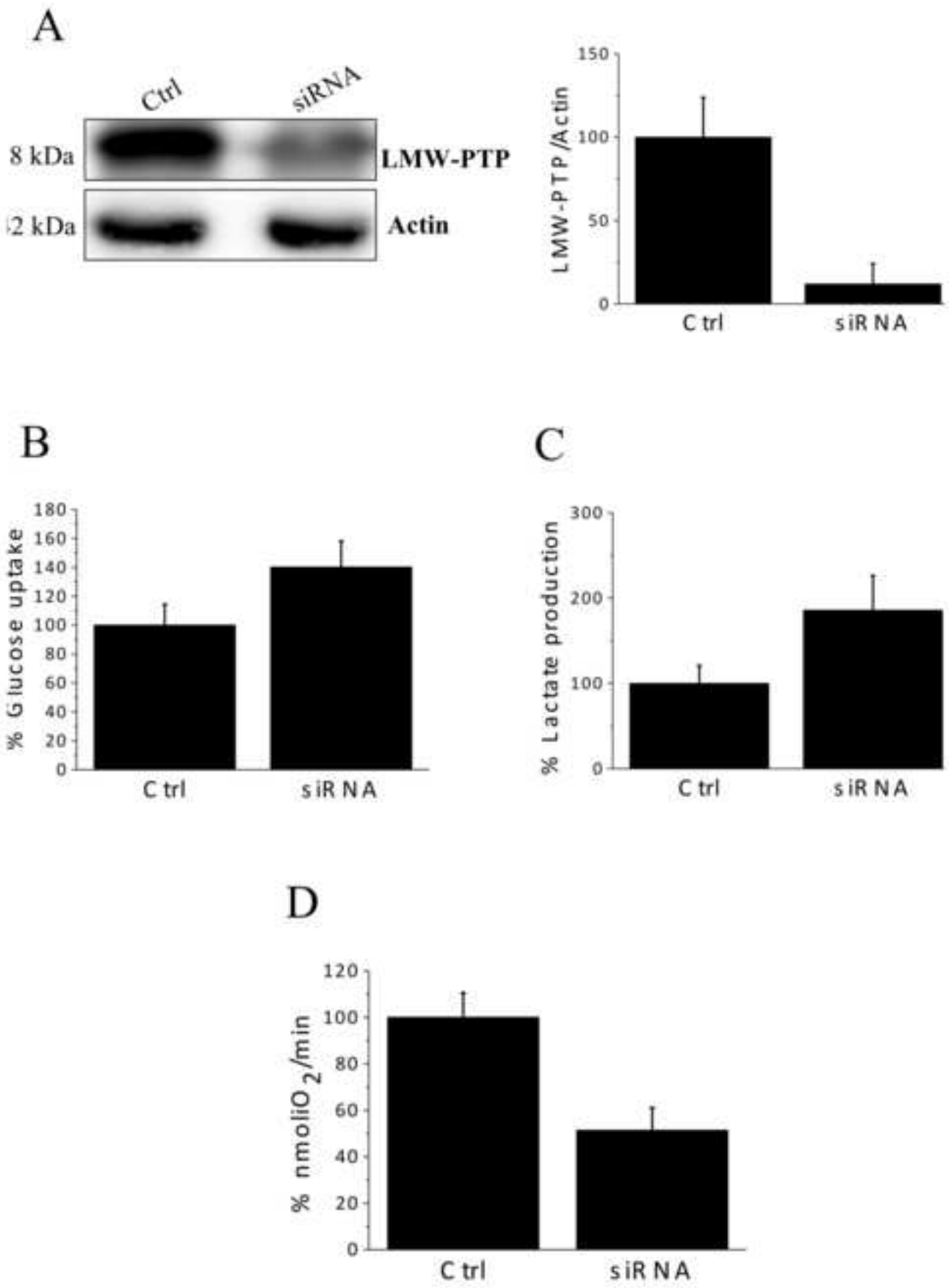

Figure S3

Click here to download high resolution image

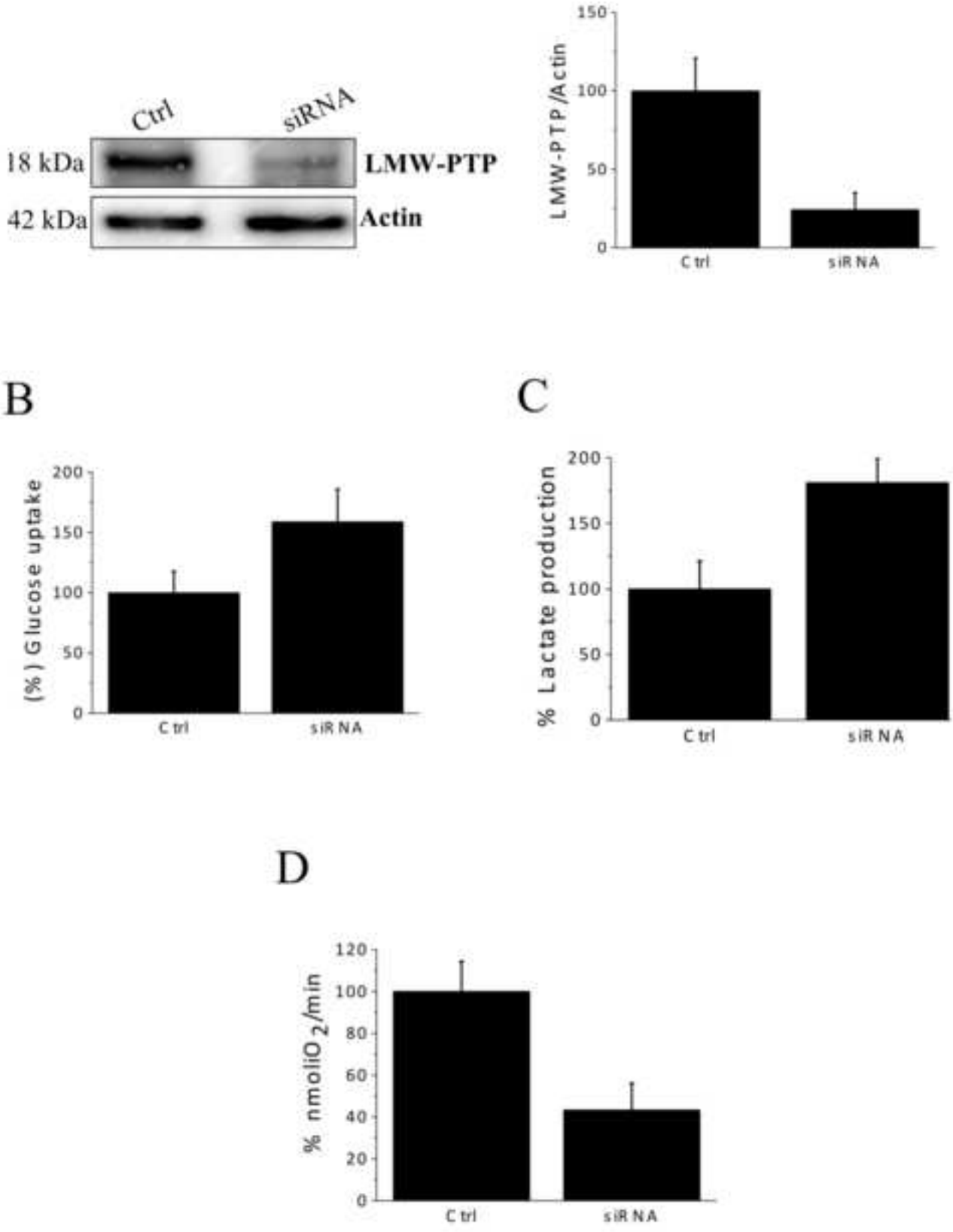

Supplementary Material (for review purposes only)
Response to reviewer 2.

Query 6*: Figure 3G: it would be nice to show that precipitation with an irrelevant antibody does not precipitate LMWPTP.*
Response 6: As suggested by reviewer, we have performed an experiment, using antibodies against GM-130 (P-20) (Santa Cruz Biotechnology SC-16268). GM 130 is a cis-Golgi matrix protein involved in vesicle tethering to Golgi membrane. Until now, no data about the interaction between GM130 and LMW-PTP was reported or published before. As showed in Figure 1 (Supplemental material for reviewers), any signal was visible after probing membrane with LMW-PTP antibodies, confirming that the interaction between PKM2 and LMW-PTP is specific. Finally, to highlight this result, we have added a sentence in Figure 3 caption.

Figure Query 6

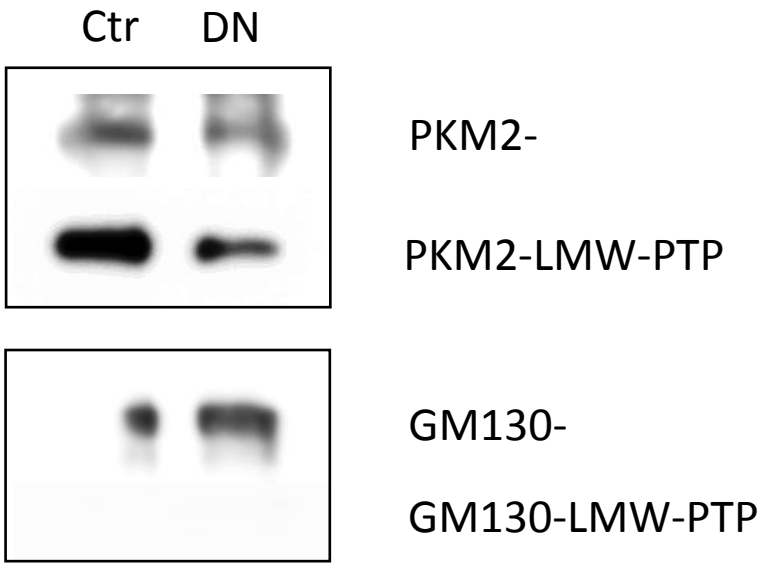

Figure Query 6: Co-immunoprecipitation analysis. A375 cells, expressing or not the dominant negative of LMW-PTP, were lysed and incubated with PKM2 or GM130 antibodies overnight. The protein A was used to precipitate antibodies and the precipitates were collected and analyzed by western blot. Membranes were probed with antibodies anti-LMW-PTP in order to verify the specificity of interaction.

Query 7*: The authors use Morin to inhibit LMWPTP, but they have themselves shown that this compound also inhibits PTP1B and TC-PTP with a lower IC50. (Cancer Med. 2018 May; 7(5): 1933-1943). Thus, PTP1B may also be involved in the results in Figure 4 and the differences between Figure 4 and Figure 5. Furthermore, cells were starved in Figure 4, and not in Figure 5, which hampers comparison. Is it not possible to treat cells longer with Morin, for a better comparison?*
Response 7: As suggested by reviewer, we performed a test with Seahorse XF analyzer incubating A375 cells with Morin for 24 hours before the analysis. The standard protocol used for Seahorse analysis forecasts seeding and treatment of cells in the same moment. Unfortunately, we observed that, after 24 hours incubation, most of cells were suffering or undergoing death. As consequence, data obtained resulted not to be comparable with the ones obtained incubating Morin for 4 hours.
Based on this evidence, we decided to change protocol, using compound 23 a novel LMW-PTP specific inhibitor (see ref. 9 of this paper, Stanford et al., 2017) to carried out a further test. In our opinion, this compound enables us to address both requests of reviewer. First, this compound is a specific inhibitor of LMW-PTP. Moreover, this compound can be used in standard growth

conditions (complete medium with FBS instead of starvation medium), enabling us to obtain data comparable with that reported in the Figure 5. Results of new experiments were reported in the Figure 2. The results of experiment carried out after 4 hours incubation, show that the treatment with compound 23 decreases basal OCR, without affecting basal ECAR. These results are in total agreement with data obtained using Morin and, suggest that data reported in the Figure 4 are really due to LMW-PTP inhibition and not to inhibition of PTP1B. A similar test was carried out incubating A375 cells in the presence of compound 23 for 24 hours. Likewise, the test carried out with Morin, we observed that most of cells are suffering or death. This evidence suggests that a technical problem prevents obtaining reproducible and analyzable results after 24-hours incubation both with Morin or compound 23. Actually, we would like not to show these results in the present paper, since a new manuscript is in preparation, concerning compound 23, in the frame of a collaboration with Dr. Bottini's group.

Figure Query 7.

A

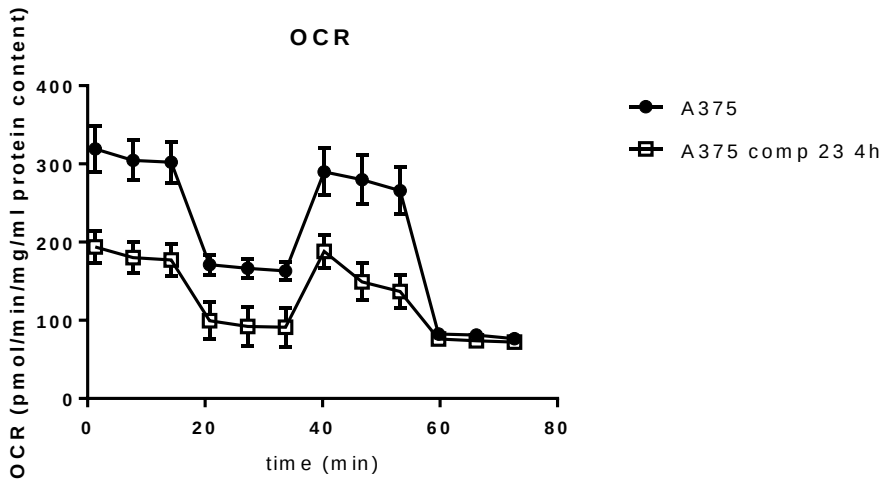

B

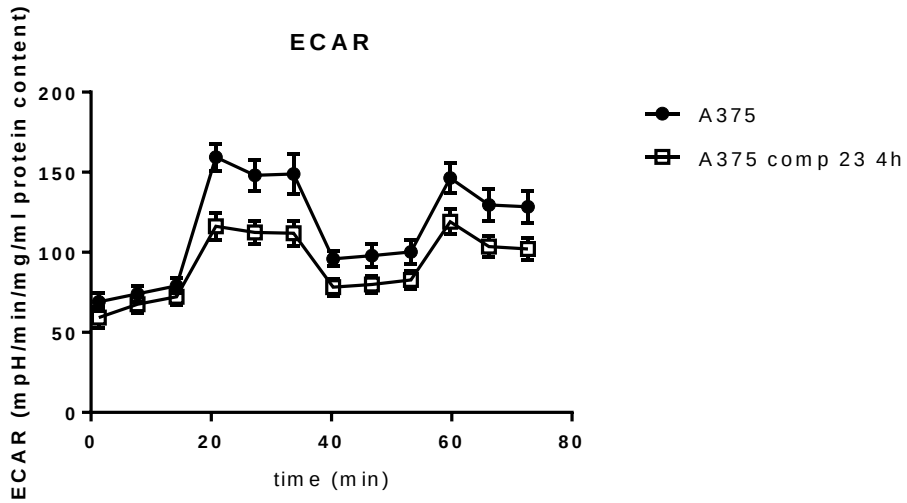

C

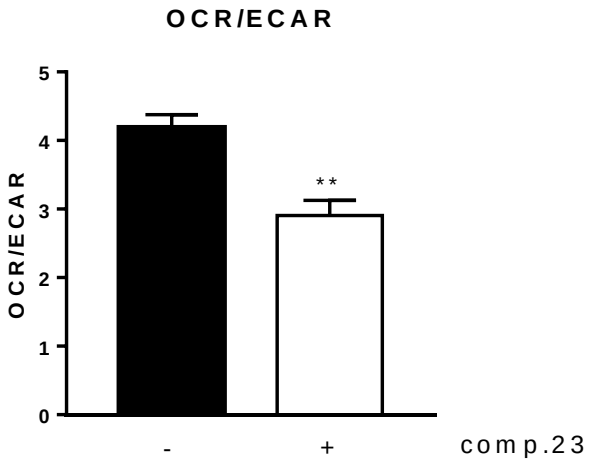

Figure Query7: Seahorse analysis of A375 cells treated with compound 23 for 4 hours. (**A**), oxygen consumption rate (OCR); (**B**) extracellular acidification rate (ECAR); (**C**), OCR/ECAR ratio in basal condition

***Conflict of Interest form**

Click here to download Conflict of Interest form: coi_disclosure.pdf